NASA Conference Publication 2157

NASA-CP-2157 19810011182

VAS Demonstration Sounding Workshop

Proceedings of a satellite
sounding workshop held July 15, 1980
at the NASA/Goddard Space Flight Center,
Greenbelt, Maryland

Edited by
Daniel L. Endres and Louis W. Uccellini

Organized by
Louis W. Uccellini, Harry Montgomery, and Daniel L. Endres

Sponsored by
The National Aeronautics and Space Administration
Operational Satellite Improvement Program (OSIP)
VISSR Atmospheric Sounder (VAS) Demonstration

NASA

NASA Conference Publication 2157

VAS Demonstration Sounding Workshop

Proceedings of a satellite
sounding workshop held July 15, 1980
at the NASA / Goddard Space Flight Center,
Greenbelt, Maryland

Edited by
Daniel L. Endres and Louis W. Uccellini

Organized by
Louis W. Uccellini, Harry Montgomery, and Daniel L. Endres

Sponsored by
The National Aeronautics and Space Administration
Operational Satellite Improvement Program (OSIP)
VISSR Atmospheric Sounder (VAS) Demonstration

National Aeronautics and
Space Administration

**Scientific and Technical
Information Office**

1980

FOREWORD

This report documents the presentations at the VAS Demonstration Sounding Workshop held at the NASA Goddard Space Flight Center on July 15, 1980. The purpose of the Workshop was to provide a forum within which a growing number of meteorologists interested in using TIROS-N and VAS data could interact with scientists responsible for developing retrieval techniques that yield satellite-derived temperature and moisture profiles. Seven papers were presented to review operational sounding techniques, discuss problems with the colocation concepts and cloud-correction techniques, evaluate TIROS-N soundings within an operational analysis scheme and FGGE special effort, and propose new techniques for retrieving moisture and temperature profiles from TIROS-N and VAS radiance measurements.

Louis W. Uccellini
VAS Demonstration Scientist
Goddard Space Flight Center

CONTENTS

OPERATIONAL SOUNDING ALGORITHMS

William L. Smith

NOAA/NESS
Madison, Wisconsin

ABSTRACT

The analytical equations used to interpret TIROS-N sounding radiances for operational applications are presented in this paper. Both the National Environmental Satellite System (NESS) Global Operational Synoptic Scale and the NESS/University of Wisconsin (UW) North America Mesoscale Sounding Production Systems are considered.

1. Introduction

The characteristics of the TIROS-N sounding system and an overview of the methods used to process the data have already been presented by Smith *et al.*, (1979). An analysis of the accuracy characteristics of the data is provided by Phillips *et al.*, (1979), Schlatter (1980) and Gruber *et al.*, (1980). Examples of the meteorological capabilities of TIROS-N for both synoptic and mesoscale applications are given by Smith *et al.*, (1980) and Hayden *et al.*, (1980). Lacking in the published references cited above is a presentation of the analytical algorithms used to convert the spectral radiance measurements into temperature and moisture profile data; therefore, these equations are presented in this paper.

2. Global Data Processing Equations

The analytics of the global sounding data processing system are those developed by Smith and Woolf (1976) for interpreting the TIROS-N prototype sounding radiance data obtained from the Nimbus-6 satellite. Eigenvectors of statistical covariance matrices of radiance, temperature, and moisture are used to formulate solutions for: (1) clear-column radiance, (2) temperature profile, and (3) moisture profile. At present the radiance, temperature, and moisture profile eigenvectors are generated from a contemporary 2-week and 4-week sample of quasi-coincident radiance and radiosonde data for the Northern and Southern hemispheres, respectively.

(a) Clear-Column Radiance

The solution for clear-column radiance from partly cloudy measurements is achieved using the "N* equation" derived by Smith (1968):

$$R_j = \frac{R_{1,j} - N^* R_{2,j}}{1 - N^*} \tag{1}$$

where R_j is the clear-column radiance for spectral channel j, subscripts 1 and 2 denote two geographical fields of view, and N* is the ratio of cloud amounts in the two fields of view. The above equation is derived under the assumption that the variation of radiance observed in two neighboring fields of view is caused solely by a variation in cloud amount. In the case of the TIROS-N HIRS radiometer, the fields of view have a nominal diameter and spacing of 30 km so that an assumption of uniform cloud type (height and opacity) is implied over areas having linear dimensions of 30 x 60 km.

The unknown variable of (1), N*, is determined using the eigenvector expansion for cloud-free-radiance:

$$R_j = \bar{R}_j + \sum_{i=1}^{N} C_i R^*_{i,j} \qquad \begin{matrix} j = 1, 2 \ldots \text{Number of Spectral Channels} \\ i = 1, 2 \ldots \text{Number of Eigenvectors} \end{matrix} \qquad (2)$$

where $R^*_{i,j}$ are the eigenvectors of a radiance covariance matrix. In the case of TIROS-N components of the radiances observed within 17 infrared channels (7–15 μm CO_2, 1–9.6 μm O_3, 1–11 μm window, 3–6.3 μm H_2O, and 5–4.3 μm CO_2) together with three microwave channels (in the 50–60 GHz O_2 band) are represented by each eigenvector. It has been found that only 10 of the 20 eigenvectors are sufficient to represent the spectral radiance distribution to within the noise level of measurements (i.e., N = 10 in (2)).

Substituting (1) into (2) yields

$$R_{1,j} - \bar{R}_j = N^*(R_{2,j} - \bar{R}_j) + \sum_{i=1}^{10} (1 - N^*) C_i R^*_{i,j} \qquad (3)$$

Since we have 20 spectral channels, (3) represents a system of 20 equations with only 11 unknowns, one of which is N*. The least squares solution of (3) is achieved by assuming that for the cloud insensitive microwave radiances, $R_{1,j} = R_{2,j} = 0.5^* (R_{1,j} + R_{2,j})$, where the microwave radiances have been interpolated to the HIRS field of view (FOV) locations.

Because of the slightly different field of view characteristics for the HIRS longwave channels (1–12) and shortwave channels (13–19), in practice we treat these two spectral regions separately, allowing for the specification of a longwave and shortwave N*. In each case the three microwave channels are used, which results in a solution of 15 equations for eight unknowns and eight equations for six unknowns for the longwave and shortwave cases, respectively.

In the global sounding operation, soundings are derived from radiances for a 9 x 6 array of HIRS FOVs and spatially interpolated radiances from the Microwave Sounding Unit (MSU). The clear-column radiance determinations for partly cloudy measurements are combined with cloud-free measurements to form a spatial average set for the area (~250 km in linear dimension) from which the sounding is to be specified. All "observed" clear and clear-column derived radiances are subjected to a variety of validity tests summarized by Smith *et al.*, (1980), before their inclusion in the averaging process.

(b) Temperature Soundings

The TIROS-N global processing system utilizes eigenvector regression. Consider expansions of both atmospheric temperature and radiant brightness temperature in terms of their empirical functions, namely

$$\vec{t} = \underset{\sim}{T}^* \vec{a}, \qquad (4)$$

$$\vec{t}_B = \underset{\sim}{T}_B^* \vec{b}, \qquad (5)$$

where $\vec{t}$ and $\vec{t}_B$ are vectors of temperature and brightness temperature deviations from sample mean values and the $\underset{\sim}{T}^*$ and $\underset{\sim}{T}_B^*$ are matrices of empirical functions, in this case the first 10 modes of eigenvectors of the temperature and brightness temperature covariance matrices. The vectors $\vec{a}$ and $\vec{b}$ are the corresponding expansion coefficients.

Usually one attempts to retrieve $\vec{t}$ and $\vec{t}_B$. However, it is easier and more stable to retrieve $\vec{a}$ from $\vec{b}$ through a transformation matrix $\underset{\sim}{D}$. That is, using least squares and the orthogonality property,

$$\vec{a} = \underset{\sim}{D}\vec{b} = \underset{\sim}{D}(\underset{\sim}{T}_B^{*T}\underset{\sim}{T}_B^*)^{-1}\underset{\sim}{T}_B^{*T}\vec{t}_B = \underset{\sim}{D}\underset{\sim}{T}_B^{*T}\vec{t}_B, \tag{6}$$

where $\underset{\sim}{D}$ is the desired transformation matrix. If $\underset{\sim}{D}$ is known, then $\vec{a}$ can be determined directly from the measured brightness temperatures (cloud-free). The $\underset{\sim}{D}$ matrix can be determined from the $\vec{a}$ and $\vec{b}$ observations corresponding to the statistical sample used to generate the eigenvectors of the temperature and brightness temperature covariance matrices. Writing (6) to cover all soundings in the sample gives

$$\underset{\sim}{A} = \underset{\sim}{D}\underset{\sim}{B}, \tag{7}$$

where the elements of matrices $\underset{\sim}{A}$ and $\underset{\sim}{B}$ are the values of the $\vec{a}$ and $\vec{b}$ coefficients for each mode and sounding. Using the least squares solution to determine $\underset{\sim}{D}$ yields

$$\underset{\sim}{D} = \underset{\sim}{A}\underset{\sim}{B}^T(\underset{\sim}{B}\underset{\sim}{B}^T)^{-1}, \tag{8}$$

where by orthogonality

$$\left.\begin{aligned}\underset{\sim}{B} &= \underset{\sim}{T}_B^{*T}\underset{\sim}{T}_B \\ \underset{\sim}{A} &= \underset{\sim}{T}^{*T}\underset{\sim}{T}\end{aligned}\right\}$$

and the matrices $\underset{\sim}{T}_B$ and $\underset{\sim}{T}$ have dimensions of the number of channels and pressure levels, respectively, by the number of soundings in the sample.

The solution for the temperature profile from a given set of brightness temperature observations is then obtained by substituting (6) in (4) to obtain

$$\vec{t} = \{\underset{\sim}{T}^*\underset{\sim}{D}\underset{\sim}{T}_B^{*T}\}\vec{t}_B = \underset{\sim}{C}\vec{t}_B \tag{9}$$

where $\underset{\sim}{C}$ is a matrix of "eigenvector regression coefficients."

In the case of TIROS-N, the eigenvector regression coefficients are obtained from a contemporary colocated sample of measured (clear-column) radiances and radiosonde observations. The samples are stratified into five latitude zones: 90–60N, 60–30N, 30N–30S, 30S–60S, 60S–90S.

Eigenvector regression coefficients are derived for levels below the 100-mb level, while ordinary linear regression is used for stratospheric levels. In order to avoid discontinuities along the latitudes used to stratify the statistical data, the regression coefficients are interpolated to specific sounding conditions using a microwave brightness temperature as the interpolation variable. In the case of extensive overcast cloud conditions, a set of microwave and stratospheric channel infrared temperature profile regression relations are used for the profile determination.

(c) Water Vapor Sounding

Water vapor mixing ratio profiles are calculated by the same method used for temperature profiles. For water vapor profiling, however, only the first three water vapor profile eigenvectors are used for specifying the water vapor profile, although all 10 radiance eigenvectors are utilized. As yet, no water vapor profiles are obtained for extensive overcast cloud conditions in the global data processing system.

3. Mesoscale Data Processing Equations

The NESS/UW man-interactive system (Smith *et al.*, 1979) for processing direct readout TIROS-N data for mesoscale applications employs a number of physics refinements not yet incorporated in the global data processing system. Included are: (1) removal of surface contribution, (2) removal of reflected solar contributions to the shortwave infrared sounding channels, (3) correction of infrared radiances for attenuation by extended cloudiness, (4) the use of synthetic radiances for generating more sensitive regression relations between radiance and temperature and moisture profiles, (5) the parameterization of the moisture profile below extended cloud in terms of the saturation mixing ratio and the amount of cloudiness.

(a) High Resolution Retrieval Method

Consider a 3 x 3 array of HIRS FOVs for which we desire a retrieval assigned a location of FOV (2, 2). A total of nine different soundings is achieved from the nine elements, one by assuming that the central element (2, 2) is clear and eight by using equation (1) and N* determinations from the radiance observed for element (2, 2) and the radiances from each of the eight elements adjacent to element (2, 2). In this case, however, N* is determined using the coefficients to a regression relation between the cloud-insensitive lower tropospheric sensing microwave channel and the clear-air radiances in the infrared:

$$R(MW) = \alpha_0 + \sum_{j=1}^{M} \alpha_j R_j. \tag{10}$$

Substituting (10) into (1) yields

$$N^* = \frac{R(MW) - \alpha_0 - \sum_{j=1}^{M} \alpha_j R_{1,j}}{R(MW) - \alpha_0 - \sum_{j=1}^{M} \alpha_j R_{2,j}}. \tag{11}$$

The "best" retrieval of the nine possible is selected through a comparison of the resulting temperature profile with a temperature sounding calculated solely from the microwave channel radiances. Using the mimimum sum of the squares criteria,

$$T(p) = T_k(p) \text{ for that k in which } \left\{\sum_p [T_k(p) - T_{MW}(p)]^2\right\} = \text{MIN.}$$

(b) Surface and Solar Radiance Removal

Since many of the lower tropospheric sounding infrared channels possess large surface contributions, the sensitivity of atmospheric temperature and moisture regression to upwelling radiance can be significantly improved by removing the surface contribution to the observed radiance. The contribution to the clear-air radiance can be estimated accurately using the water vapor corrected 11 μm window brightness temperature. The remaining atmospheric contribution to the observed radiance is then

$$A_j = R_j - B(\nu_j, T_s)\, \tau\, (\nu_j, p_s), \tag{12}$$

where B is the Planck radiance and the surface temperature, T_s, is estimated from the 11 μm brightness temperature. The transmittance of the atmosphere, $\tau\ (\nu_j, p_s)$ is computed from a regression estimate of the temperature and water vapor profile obtained from the microwave radiance data and in-situ surface pressure, temperature, and dewpoint observations. Removal of the surface contribution to the observed radiances reduces the standard error of the regression estimates of temperature and dewpoint by as much as 20 percent and 70 percent, respectively (Hayden *et al.*, 1980).

Reflected sunlight also contributes to the radiances in the 3.7 – 4.6 μm region. It can be removed by assuming that the reflectivity of the reflecting surface is constant between 4.0 and 4.6 μm. Since the solar contribution to the radiance in any channel, ν, is

$$SC(\nu) = B(\nu, 5800K)\, \Omega_s\, \tau^{\gamma}\, (\nu, p_s)\, \tau_{\beta}\, (\nu, p_s)\,, \tag{13}$$

where Ω_s is the solid angle subtended by the sun, r_s is surface reflectivity, and $\gamma = \sec\phi_0$ and $\beta = \sec\phi$ where ϕ_0 and ϕ are solar zenith angle and satellite viewing zenith angle, respectively. The ratio of solar contributions for two channels is

$$\frac{SC(\nu)}{SC(\nu_0)} = \frac{B(\nu, 5800K)}{B(\nu_0, 5800K)} \left[\frac{\tau(\nu, p_s)}{\tau\,(\nu_0, p_s)}\right]^{\sec\phi_0 + \sec\phi}, \tag{14}$$

respectively. Using the 4.0 μm window for the reference channel (ν_0), then

$$SC(\nu_0) = R(4.0\ \mu m) - B(4.0\ \mu m, T_s), \tag{15}$$

where T_s is given by the 11 μm window channel brightness temperature. Combining (15) with (14)

enables the solar contamination for all 4.3 μm sounding channels to be estimated and subtracted from the clear-air radiance observations prior to their use for the profile estimation.

(c) Overcast Cloud Retrieval

If the 3 x 3 array of FOVs used in an attempt to determine the clear-air radiances is heavily clouded, as can be determined from the observed radiances, then a single FOV cloud correction algorithm is employed (Smith, Woolf, and Jacob, 1970). Assuming a single level of cloud, it can be shown that the attenuation of the measured radiance, R_m, by cloud is

$$C(\nu) = [R(\nu) - R_m(\nu)] = \epsilon(\nu) \int_{p_c}^{p_s} \tau(\nu, p) \frac{dB(\nu, T)}{dp} dp, \tag{16}$$

where $\epsilon(\nu)$ is the effective emissivity of the cloud and p_c is the cloud pressure. Assuming that $\epsilon(\nu)$ in the 11–15 μm region is constant, we can write

$$\frac{R(\nu_r) - R_m(\nu_r)}{B(11\ \mu m, T_s) - R_m(11\ \mu m)} = \frac{\int_{p_c}^{p_s} \tau(\nu_r, p) \frac{dB(\nu_r, T)}{dp} dp}{B(11\ \mu m, T_s) - B(11\ \mu m, T_c)}. \tag{17}$$

Given an estimate of the temperature and water vapor profile from the microwave radiance data and surface observations, p_c can be determined from (17) using the most transparent 15 μm CO_2 channel (13.4 μm as ν_r). Having determined p_c, $\epsilon(\nu)$ is determined from (16) using the 11 μm window channel to determine an $\epsilon(\nu_L)$ for the longwave infrared channels and the most transparent 4.3 μm CO_2 channel (4.57 μm) to determine an $\epsilon(\nu_s)$ for the shortwave infrared channels. Cloud corrections for all other sounding channels are then determined from (16). The cloud-corrected radiances can then be used as clear-column radiances in the solution for the temperature and moisture profiles. The cloud correction process can be iterated if necessary.

During the day it is necessary to determine the contribution to the short-wave channels due to reflection of sunlight by the clouds. In this case it is assumed that $\epsilon(\nu_s) = \epsilon(\nu_L)$. The solar correction for the 4.57 μm channels ($\nu = \nu_s$) is expressed by

$$SC(\nu_s) = R_m(\nu_s) + \epsilon(\nu_L) \int_{p_c}^{p_s} \tau(\nu_s, p) \frac{dB(\nu_s, \hat{T})}{dp} dp - R(\nu_s), \tag{18}$$

where T denotes the estimated temperature profile. The solar correction for all other shortwave channels can then be shown to be

$$SC(\nu) = SC(\nu_s) \frac{B(\nu, 5800K)}{B(\nu_s, 5800K)} \left[\frac{\tau(\nu, p_c)}{\tau(\nu_s, p_c)}\right]^{(\sec\phi_0 + \sec\phi)} \tag{19}$$

The final value of the daytime "overcast" cloud-corrected radiance with surface and solar contributions removed is

$$R^1(\nu) = R_m(\nu) + \epsilon(\nu) \int_{p_c}^{p_s} \tau(\nu, p) \frac{dB(\nu, T)}{dp} dp - B(\nu, T_s)\, \tau(\nu, p_s) - SC(\nu). \quad (20)$$

(d) Cloudy Parameterization of Moisture

In the clear or partly cloudy atmosphere, the moisture profile is obtained from the infrared H_2O absorption channels. However, in heavily clouded regions, these channels are insensitive to the moisture below the cloud. As a result, it is necessary to parameterize the moisture profile below the cloud on the basis of the saturation mixing ratio and the expected clear air value at the cloud level, surface mixing ratio, and effective cloudiness, $\epsilon(\nu_L)$. In this case the mixing ratio at the cloud level is assumed to be

$$W(p_c) = \epsilon(\nu_L) W_{sat}(T_c) + [1 - \epsilon(\nu_L)] W_0 \left(\frac{p_c}{p_0}\right)^3 , \quad (21)$$

where the zero subscript refers to surface conditions. The profile between cloud and ground is then

$$W(p) = W_0 \left(\frac{p}{p_0}\right)^{\lambda} \qquad \text{with } \lambda = \frac{\ln[W(p_c)/W_0]}{\ln(p_c/p_0)} . \quad (22)$$

The parameterized water vapor profile is used below cloud level to calculate the transmittance function required to obtain the cloud corrections and surface contributions to the measured radiances.

(e) Use of Synthetic Regression

Due to time and space discrepancies of colocated samples of radiance and radiosonde data, the noise associated with real data regression is excessive, resulting in conservative regression relations (i.e., they are less sensitive than they should be). This problem is alleviated using radiances "synthesized" by radiative transfer calculation from the observed radiosondes. Accurate synthesization depends on correct specifications of the transmittance functions, $\tau(\nu, p)$, and the noise level of the radiances with respect to sounding determination, including both instrumental and atmospheric noise sources.

The colocated radiance/radiosonde sample can be used to empirically correct theoretically-based transmittances and to specify the noise level of the observations. Assuming that $\tau_T(\nu, p) = \tau^{\gamma}(\nu, p)$, where the subscript T denotes a true value, then we can solve for that γ for each channel which minimizes the quantity

$$S_{\gamma}(\nu) = \frac{1}{N} \sum_{N} [R_{\gamma}(\nu) - R(\nu)]^2 . \quad (23)$$

Having determined γ, it is reasonable to assume that the expected noise $\eta(\nu)$ is given by

$$\eta(\nu) = \sqrt{fS_{\gamma}(\nu)} \ , \tag{24}$$

where the factor f must be less than unity due to "mismatch noise." It has been found from experience that the best retrieval results are achieved by assuming that f = 1/4.

Given $\gamma(\nu)$ and $\eta(\nu)$, a statistically representative set of radiance observations can be generated from a statistically representative set of radiosonde data. In the NESS/UW mesoscale processing system, several weeks of profile data from a standard set of 28 North American and Caribbean radiosonde stations are used to generate profile retrieval regression relations using the corresponding TIROS-N radiances synthesized from the profile data.

4. Summary and Further Remarks

The current global operational sounding algorithms are linear and statistical. Improvements have been demonstrated in the mesoscale sounding process by accounting for physical processes such as surface contributions, which may be uncorrelated with atmospheric emission, reflected solar contributions, and cloud attenuation. Improved solution sensitivity can be achieved using regression relations based on radiosonde-synthesized radiances rather than actual radiance observations, since actual observations are imperfectly registered in time and space with radiosonde observations.

The main limitation of current operational sounding methods is that they rely on contemporary radiosonde data for obtaining the solution coefficients. The ultimate retrieval method should be a completely physical/analytical solution of the radiative transfer equation so that retrieval variations in time and space can be attributed entirely to variations in the measured radiances. Complete physical solutions do not yet yield accuracies comparable to statistical solutions as measured through comparisons of retrievals with radiosondes. However, satellite sounding independence of radiosonde data may be a more important quality than their RMS difference with radiosonde data. Current emphasis should be placed on implementing radiosonde-independent sounding retrieval methods which yield accuracies comparable to those achieved with the current radiosonde-dependent methods.

References

1. Gruber, A., H. Brodrick, and C. Watkins, 1980: Evaluation of sounding data obtained from TIROS-N and NOAA-6. Presented at the International Conference on Preliminary FGGE Data Analysis and Results, Bergen Norway, June 23-27.

2. Hayden, C. M., W. L. Smith, and H. M. Woolf, 1980: Determination of moisture from NOAA polar orbiting satellite sounding radiances. Presented at the International Conference on Preliminary FGGE Data Analysis and Results, Bergen Norway, June 23–27.

3. Phillips, N., L. McMillin, A. Gruber, D. Wark, 1979: An evaluation of early operational temperature soundings from TIROS-N. *Bull. Am. Meteor. Soc.*, 60, pp. 1188–1197.

4. Schlatter, T. W., 1980: An assessment of operational TIROS-N temperature retrieval over the United States. Accepted for publication in the *Mon. Wea. Rev.*, Vol. 108.

5. Smith, W. L., 1968: An improved method for calculating tropospheric temperature and moisture from satellite radiometer measurements. *Mon. Wea. Rev.*, 96, pp. 387–396.

6. ____, H. M. Woolf, and W. Jacob, 1970: A regression method for obtaining real time temperature and geopotential height profiles from satellite spectrometer measurements and its application to Nimbus-3 "SIRS" observations, *Mon. Wea. Rev.*, 98, pp. 582–603.

7. ____, and H. M. Woolf, 1976: The use of eigenvectors of statistical covariance matrices for interpreting satellite sounding radiometer observations. *Journal of the Atmospheric Sciences*, 33, pp. 1127–1140.

8. ____, H. M. Woolf, and C. M. Hayden, 1979: The TIROS-N operational vertical sounder. *Bull. Am. Meteor. Soc.*, 60, pp. 1177–1187.

9. ____, F. W. Nagle, C. M. Hayden, and H. M. Woolf, 1980: Vertical mass and moisture structure from TIROS-N. Presented at the 23rd COSPAR Conference, Budapest Hungary, June 2–14.

IMPROVEMENTS TO SATELLITE RETRIEVAL SYSTEMS: THE OPERATIONAL PERSPECTIVE

Larry McMillin
NOAA/NESS
Silver Spring, Maryland

1. Introduction

Atmospheric temperature profiles have been determined from radiances measured on operational satellites since shortly after the launch of NOAA-2 on October 15, 1972. Although the operational satellite had been preceded by several experimental satellites, it was soon learned that many of the procedures that had worked on experimental cases needed to be modified in an operational situation. Perhaps one of the biggest differences is the emphasis on soundings with large errors. While these may be manually edited in an experiment, they frequently play a large role in the credibility of operational soundings. Thus, the early portion of the life of a satellite system is characterized by frequent changes to the operational mode.

Operational weather satellites are built as a series of nearly identical instruments, which are flown for 5 to 7 years. Minor improvements are made during the life of the series. However, major improvements and changes in design are made with the initiation of a new series of instruments. Similarly, procedures used to process the data are characterized by frequent changes early in the life of a satellite series as user experience is gained with the new instrument. Later the changes become less frequent, both because the processing system becomes well tuned to that particular set of instruments and because, at the end of a series, resources are devoted to generating the processing system for the next set of instruments.

To illustrate this process, it is helpful to discuss the present and past systems. The Vertical Temperature Profile Radiometer (VTPR) was used to produce operational soundings from October 15, 1972 until March 1, 1979. On that date, the operational soundings were switched to the TIROS-N Operational Vertical Sounder (TOVS) instruments, which were launched on the TIROS-N satellite on October 13, 1978. This series will last to the middle or late 80s, at which time a more advanced microwave instrument will be added.

The growth of capability is represented by the number of channels. The VTPR had eight channels, six of which determined atmospheric temperature, one determined surface temperature, and the final one determined water vapor. The TIROS-N Operational Vertical Sounder contains a total of 27 channels instead of the eight on the VTPR instrument.

One of the TOVS instruments, the High Resolution Infrared Radiometer Sounder (HIRS), has 20 channels, a subset of which duplicates the ability of VTPR. HIRS has seven channels that measure

temperature in the spectral region used by the VTPR plus five channels in a second spectral region. It also has the same window channel plus two more and three water vapor channels rather than one. In addition, it has a channel in the visible region and another channel for ozone. The second TOVS instrument is a Microwave Sounding Unit (MSU) which, in contrast to the HIRS and VTPR, is not affected by most clouds. The Third TOVS instrument is the Stratospheric Sounding Unit (SSU), which senses the upper atmosphere.

More information about the TOVS and VTPR are given in the descriptions by Smith *et al.* (1979) and McMillin *et al.* (1973), respectively. Future instruments are still being planned, but it is fairly certain that the next series will carry a microwave instrument that greatly exceeds the capability of the four-channel MSU.

At the present time, we are in the early phase of the TOVS instrument series and are still learning the characteristics of the instrument and data processing system. As a result, there are many possible improvements to test. Since the present system uses coincident radiosondes to determine empirical coefficients, the final result of a change is not known until the empirical coefficients are adjusted to the change. This can take several weeks. Also a system can run several days or even weeks without encountering conditions that cause a catastrophic error. This type of failure is acceptable in research but not in an operational mode. To protect against these failures, both testing procedures and the operational system must be more elaborate than a similar experimental system. The final result of these considerations is that the testing of a single modification requires much time and, particularly in the early life of a system, possible modifications accumulate at a faster rate than they can be tested. Thus, we have a list of desired changes and an order in which to test these changes.

One result of this continuing development is that evaluations of satellite soundings can become outdated rather rapidly. By the end of the VTPR series, both the histogram technique used to determine clear radiances and the minimum information retrieval method as described in McMillin *et al.* (1973) had been changed. One of the current features of satellite soundings is a tendency to produce conservative estimates, that is to bias all temperatures toward the mean value. This tendency is due to the method used to convert radiances to temperature and is not an inherent characteristic of satellite soundings. When the processing system is changed, this characteristic will change too. Thus, features that are characteristic of satellite soundings at a particular time when soundings were being processed in a certain way are often indications of problems in the processing system on the ground rather than problems with satellite soundings in general.

To understand the processing system being used for TOVS data, it is necessary to know the history of the system. The prototype for the HIRS was flown on Nimbus-6 and processed in a quasi-operational mode by a group of research scientists. This processing produced the experience with the enhanced capabilities of the TOVS system. At the same time, operational personnel were obtaining experience in operational procedures with the VTPR instrument. To assure completion of a system by the scheduled launch data of TIROS-N, it was decided to base the initial TIROS-N processing system on the Nimbus-6 system, and to later modify it to take account of operational

experience. Time did not allow the blending of these two areas of experience before launch so the initial TOVS system was, in some respects, inferior to the system used for VTPR data. As a result, there was a list of proposed changes for the initial TOVS system before the satellite was launched.

2. Specific Improvements

Much of the improvement that occurred during the life of the VTPR system resulted from a better understanding of the problems caused by multiple layer clouds. These problems are described by McMillin (1978, 1980) and need be only summarized here. Since infrared radiation (which produces the temperature information on present satellites) does not penetrate clouds, clear-column radiation measurements are required to produce reliable temperatures. Clear areas can be easily identified and accurate retrievals produced with the current operational system.

The problem is that for current instruments, which "see" an area 20 to 30 km wide, the number of clear areas is small and tend to be clustered in areas of little meteorological activity where one or two soundings can produce as much information as 10 or 20. Areas which are of meteorological interest are either cloudy or partly cloudy and are missed. If an area is partly cloudy, it is possible to derive a clear radiance provided that two spots can be found where cloud amount differs but where other parameters such as temperature, water vapor, surface temperature, and cloud height are the same.

The most difficult assumption to satisfy is cloud height. Consider an area of clouds of uniform size. Usually clouds are shaped more like half of an egg than a rectangle. If only a small portion of the viewing area is filled with cloud, the clouds being viewed will be mostly cloud edges. A spot that is more cloudy will contain more cloud centers. Thus, an area that is nearly clear has a lower average cloud height than one that contains more clouds. This means that accurate soundings can be obtained only in areas of shallow clouds where the error due to the different cloud heights is small. In practice, the limitation is not that restrictive because techniques already exist for selecting an area with similar average cloud heights from a group of scan spots (see McMillin, 1978).

Errors caused by the failure to allow for different cloud heights are large. In addition, they are, for a particular algorithm, all in one direction. Thus, simple averaging does not remove the error and procedures for identifying the erroneous estimates are important. Different clear-radiance techniques, which extract clear radiances from a sample of cloud-contaminated values, differ both in their selectivity and in their yield. For those cases where the required corrections are small, all techniques are reasonably accurate and there is little difference between techniques. As the yield increases, more difficult areas are included and the difference between techniques becomes apparent. These more difficult areas are more important than is indicated by their numbers, because they are located in areas where significant meteorological features occur and where gradients are large. Another factor to consider is that errors in numerical forecasts are often larger in baroclinic areas where clouds exist than in clear high pressure areas. The error level at which a satellite sounding ceases to provide useful information is frequently higher in the areas of large

forecast error and is larger than the average error level for the entire globe. The final result is that a comparison of clear radiance techniques must consider coverage as well as the error level of the two techniques and that increased coverage at the cost of a slightly higher error level is often desirable.

The TIROS-N satellite carries instruments which provide two estimates of clear-column radiances in partly cloudy areas. In the first method, the measured microwave radiance is converted to an "equivalent radiance" in the 15 μm region by first using the Planck equation to determine a radiance temperature from the microwave measurement and then using the radiance temperature to calculate an equivalent radiance in the 15 μm region. We will call this equivalent radiance $I(\nu_1, \nu_2)$ where ν_1 is in the 15 μm region and ν_2 is the microwave value. Using clear radiance only, we find the values of a_i such that

$$I(\nu_1, \nu_2) = a_0 + \sum_1^n a_i \, I(\nu_i), \tag{1}$$

where $I(\nu_i)$ are radiances in the 15 μm region. In cloudy areas, each $I(\nu_i)$ is a linear function of cloud amount. As a result, the value of $I(\nu_1, \nu_2)$ given by (1) is also linearly related to cloud amount. Thus, the value of $I(\nu_1, \nu_2)$ given by (1) is a cloudy value, and the value obtained directly from the microwave measurement is a clear estimate of the same value. Given two cloudy values of $I(\nu_1, \nu_2)$ from adjacent scan spots and the clear value for the area, the value of N* can be determined from

$$N^* = \frac{I_{c1}(\nu_1, \nu_2) - I_1(\nu_1, \nu_2)}{I_{c1}(\nu_1, \nu_2) - I_2(\nu_1, \nu_2)}, \tag{2}$$

where $I_{c1}(\nu_1, \nu_2)$ is derived from the microwave value and $I_1(\nu_1, \nu_2)$ and $I_2(\nu_1, \nu_2)$ are obtained from (1). Once the value of N* is obtained, it can be applied to the other channels.

The second method is similar except that it uses a 4.3 μm radiance in place of the microwave value. It also differs in that the 4.3 μm channel also responds to clouds so a clear value is not directly measured. Values for two scan spots establish a linear relationship between the 4.3 μm value and the values of $I(\nu_i)$ such that for any arbitrary value of the 4.3 μm channel, corresponding values of $I(\nu_i)$ are determined. These in turn are used in (1) to determine an estimate of the 4.3 μm value. Due to the nonlinear relationship between the 4.3 and 15 μm regions, the estimated and observed 4.3 μm values agree for the clear value of the 4.3 μm channel, because the coefficients, a_i, are valid only for clear conditions. Although the method could be applied to any channel, it should be applied to a channel with a uniform clear value that responds to clouds. Because a window channel responds to strong horizontal gradients which are present in the surface, a lower atmospheric channel is used that is less sensitive to the surface temperature but still responds to clouds.

The final solution is obtained by iteration of the equation

$$I(4.3)_{new} = [I'(4.3) - (\Delta I'(4.3)/\Delta I(4.3)) \times I(4.3)]/[1 - \Delta I'(4.3)/\Delta I(4.3)], \tag{3}$$

where all values on the right hand side are previous values, $I'(4.3)$ is the value calculated from (1), $I(4.3)$ is either a measured value for the first iteration or the value of $I(4.3)_{new}$ given by the previous iteration, and $\Delta I'(4.3)/\Delta I(4.3)$ is the derivative at the value of $I(4.3)$. The solution to (3) is iterative because the solution is nonlinear and the value of $\Delta I'(4.3)/\Delta I(4.3)$ is a function of the value of $I(4.3)$. When the solution converges, values of $I_{cl}(4.3)$, $I_1(4.3)$, and $I_2(4.3)$ are used in place of $I_{cl}(\nu_1,\nu_2)$, $I_1(\nu_1,\nu_2)$, and $I_2(\nu_1,\nu_2)$, respectively, in (2) to calculate N*, which is then applied to all channels. The two values of N* are averaged to get a single value. However, if they do not agree, no value is calculated and both are assumed to be wrong.

Actually, the methods used to calculate N* are not nearly as important as the procedures used to identify the bad estimates that frequently occur. Radiances for individual spots are subjected to various tests. First, the spots in a 3 x 3 array are checked for uniformity of cloud height using the procedure described by McMillin (1978). Then the two estimates of N* (one using the 4.3 μm measurement and one using the microwave measurement) are checked for consistency. Then various relationships of the form of (1) are used to determine if the 15 μm measurements are consistent with measurements in the 4.3 μm and microwave regions. Finally, the various individual estimates are checked for consistency and outliers are discarded. In a 9 x 8 array of scan spots with surrounding borders, there are 72 possible clear-radiance estimates, but some will have been deleted by previous tests. If the number remaining becomes too small or if too many of the remaining are discarded, no clear-radiance value is produced. However, if the variance of the sample is within specified limits, the values are averaged to determine the final estimate. The value is assigned to the average location of the points used to calculate the average radiances.

The effect of the clear-radiance algorithm is best shown by Figures 1 and 2, which show average errors for the three retrieval paths. The clear retrievals are obtained from observed clear radiances, while the N* retrievals are obtained from the process just described. Figure 1 shows results from the operational method that evolved from Nimbus-6 (see Smith *et al.* 1976) while Figure 2 shows results from the procedure described in this paper. Temperature retrievals for both the clear and N* paths are obtained from a single set of coefficients, so differences are due to differences in the radiances. Figure 1 shows significant differences between the clear and N* retrievals. For example, at 1000 mb, they differ by 2K. In Figure 2, the two methods show the same bias. Figures 1 and 2 show that the method described in this paper derives clear radiances that are in agreement with values observed in clear areas, while the former method derived radiances that were cold at 1000 mb and warm at 350 mb.

Other changes to the system are being considered. One involves the loss of variance that has been observed in satellite soundings. A major factor in the reduced variance is the tendency for regression to produce estimates weighted toward the mean when the predictors are subject to errors. This problem is discussed by McMillin and Dean (1980). They found that modifications to the regression procedure resulted in significant increases in the variance of the predicted temperatures. This finding demonstrates that the loss of variance can be substantially reduced.

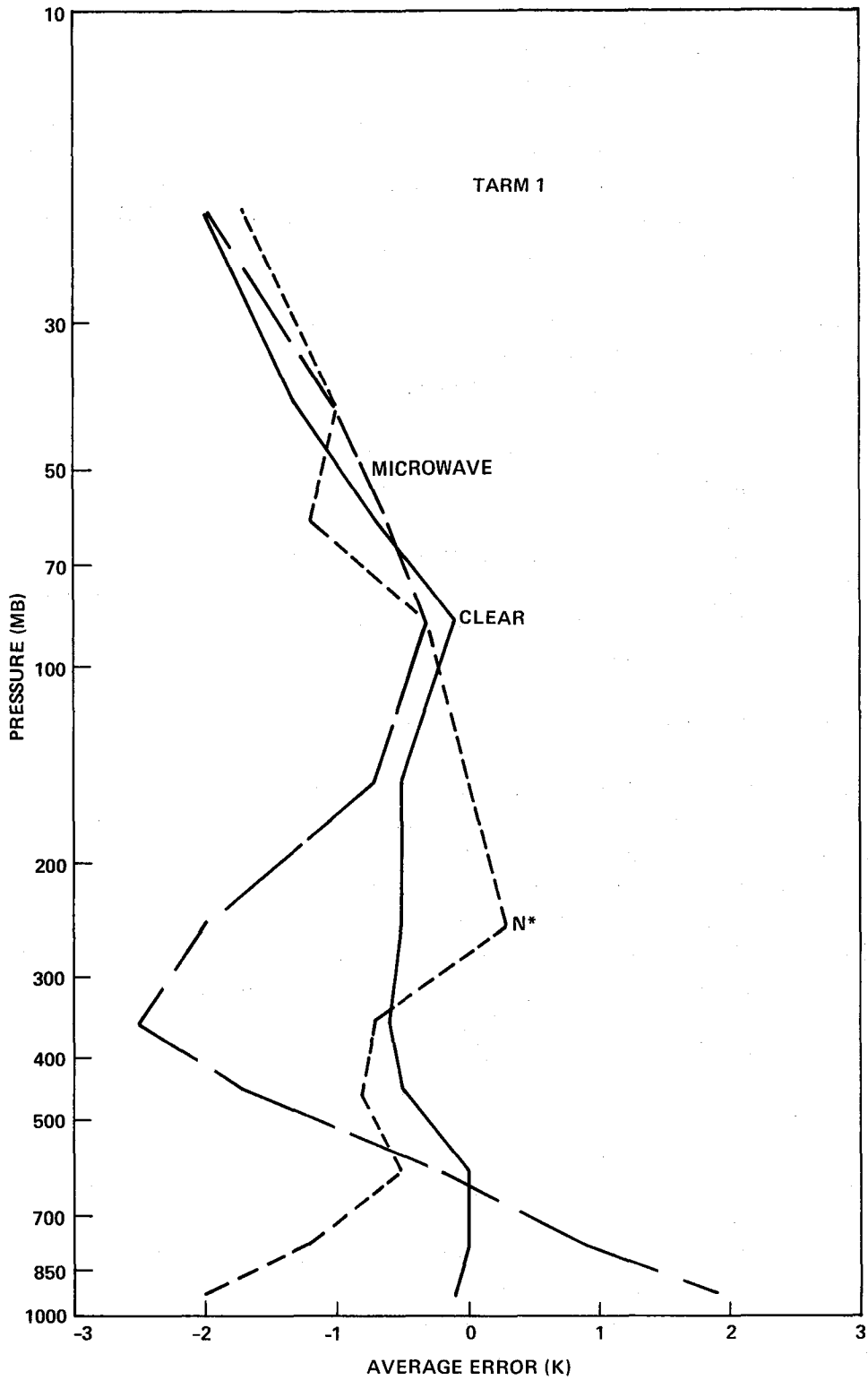

Figure 1. Average errors as a function of pressure for the TARM 1 module.

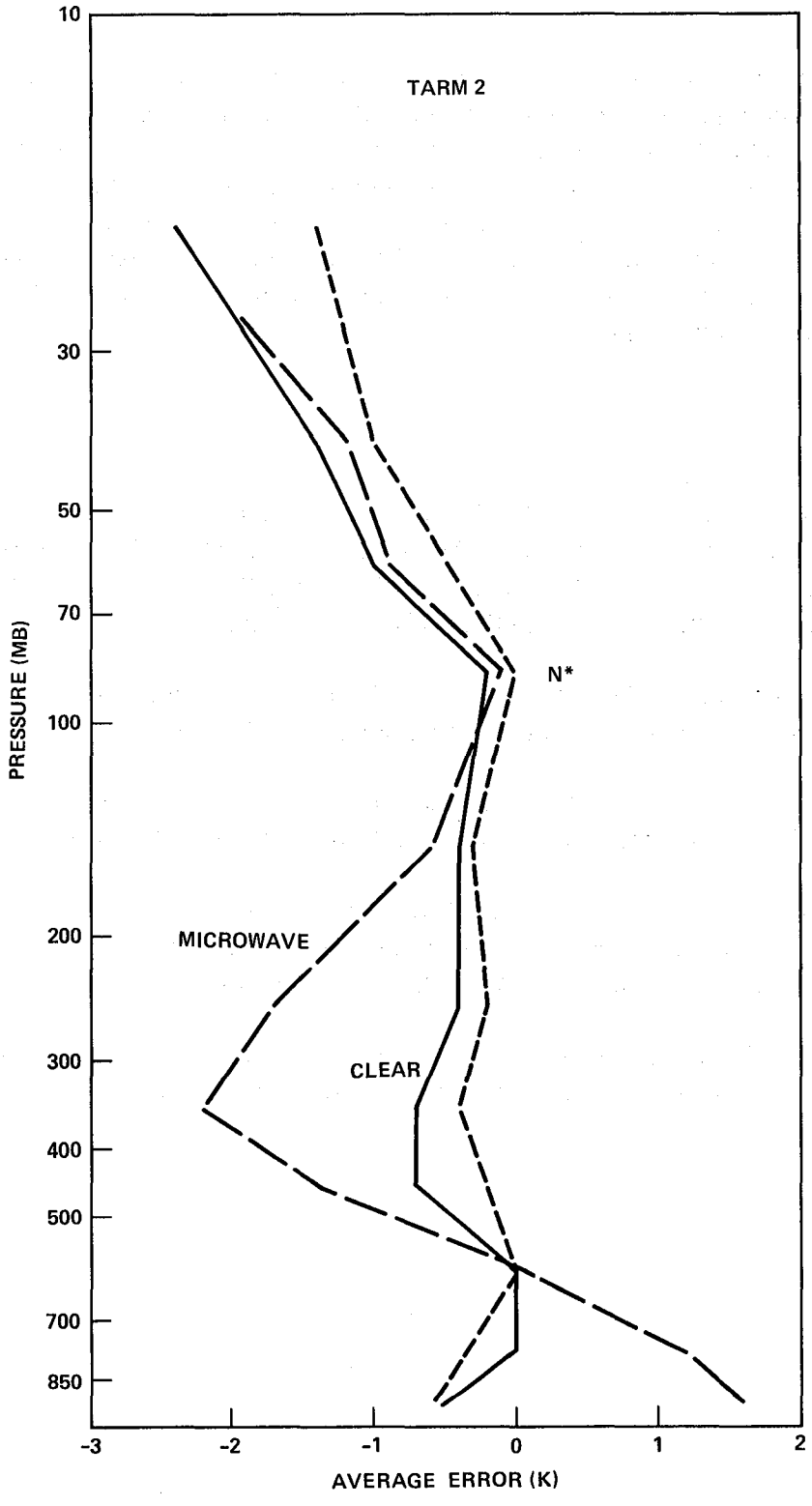

Figure 2. Average error as a function of pressure for the TARM 2 module.

3. Summary

In summary, it should be recognized that there are considerations for an operational sounding system that do not apply to a research situation. In addition, atmospheric sounding is a developing technology. Several of the speakers in this workshop are proposing very different techniques from what they were proposing 2 or 3 years ago. Two or 3 years from now, they will be proposing different techniques and striving to get those techniques into whatever systems are operational at that time. The new procedure that has been discussed for deriving clear radiances was developed for use in an operational sounding system. It is fast, accurate, and reliable. It should be used to derive soundings in partly cloudy areas.

References

1. McMillin, L. M., D. W. Wark, J. M. Siomkajlo, P. G. Abel, A. Werbowetzki, L. A. Lauritson, J. A. Pritchard, D. S. Crosby, H. M. Woolf, R. C. Luebbe, M. P. Weinreb, H. E. Fleming, F. E. Bittner, and C. M. Hayden, 1973: "Satellite Infrared Soundings from NOAA Spacecraft," NOAA Technical Report NESS 65, 112 p.

2. McMillin, Larry M., 1978: "An Improved Technique for Obtaining Clear Radiances from Cloud-Contaminated Radiances," *Mon. Wea. Rev., 106,* No. 11, 1590-1597 pp.

3. Smith, W. L., H. M. Woolf, C. M. Hayden, D. Q. Wark, and L. M. McMillin, 1979: "The TIROS-N Operational Vertical Sounder," *Am. Met. Soc., 60,* No. 10, 1177-1187 pp.

4. McMillin, L. M., and C. Dean, 1980: "An Improved Operational Technique for Eliminating Cloud Effects from Satellite Temperature Soundings," being given at the International Radiation Symposium, given at Fort Collins, Colorado.

5. McMillin, L. M., and C. Dean, 1980: "Variance Ratios, Loss of Energy, and Regression in Satellite Temperature Retrievals (submitted to *Mon. Wea. Rev.*).

EVALUATION AND USE OF TOVS RETRIEVALS AT NMC

Norman A. Phillips
NMC
Washington, D.C.

1. Introduction

In a current analysis procedure at the National Meteorological Center (NMC), a *first guess* analysis (from the latest 6- or 12-hour forecast) is updated by new data. In our newest analysis procedures based on optimum interpolation, the observational correction depends on the size of pre-assigned, expected observational errors versus the size of expected errors in the first guess forecast. In the case of Northern Hemisphere Ocean temperatures, the latter are around 2 degrees. The infrared satellite retrievals have a similar size "error." If (as assumed) their errors are uncorrelated with the first guess error, they will improve the analysis. The larger errors of the microwave retrievals, however, mean that they will be given little weight in the analysis. An evaluation of the TIROS-N retrievals is currently underway at NMC to determine the impact of satellite-derived data within operational analysis schemes, to isolate possible problems within current retrieval methods, and to offer possible solutions for these problems.

2. Evaluation of TIROS-N Retrievals

The major emphasis at NMC since March 1979, when TIROS-N data was first used at NMC, has been on oceanic temperature retrievals. Over-land retrievals have not been used yet, and the final step in judging the usefulness of oceanic water vapor retrievals has not been made (Phillips, *et al.*, 1979; Phillips and Desmarais, 1979). Tables 1, 2, and 3 demonstrate the differences in mean layer virtual temperatures in the "troposphere" obtained from TIROS-N and oceanic radiosondes for February 1979 and August 1979. Both infrared ("clear") and microwave ("cloudy") results are shown. At many layers the mean difference (bias) is larger than would be obtained by simple sampling theory where the mean difference (std dev) $= (1/\sqrt{n})\sqrt{\text{variance of difference}}$. For example, in Table 1:

$$|-2.1^\circ| > (1/\sqrt{45})\sqrt{(2.9)^2 - (2.1)^2} = 0.3.$$

More specifically, in the cloudy extratropical Northern Hemisphere case (bottom half of Table 3), the bias is large and changes sign with season. All stations in the collection show this effect, and it appeared again this past winter (1979-1980) and in the present summer (1980).

There seems to be a pervasive weakness, meteorologically and/or computationally, in the NESS statistical colocation method, which utilizes selected radiosonde observations (RAOB) data sets

Table 1
Sat–RAOB Comparison of Three Southern Hemisphere Islands (40–50S)

LAYER	RETR.	$\overline{SAT} - \overline{RS}$	RMS DIFF.	SAT. VAR. / RS. VAR.	DATES AND APPROX. PERCENTAGE
1000 – 850		1.2°	2.7°	0.9	
850 – 700	C	-0.1	1.5	0.8	JAN 30
700 – 500	L	-1.1	1.8	0.8	–
500 – 400	E	-1.4	2.2	0.8	FEB 28
400 – 300	A	-1.4	2.0	0.7	(42)
300 – 200	R	-0.6	2.0	0.3	
200 – 100		-0.1	2.0	0.5	
1000 – 850		0.0°	1.6°	1.0	
850 – 700	C	0.2	1.4	1.0	JUL 24
700 – 500	L	0.3	1.2	1.0	–
500 – 400	E	-0.7	1.8	0.9	AUG 22
400 – 300	A	-1.1	2.3	0.6	(33)
300 – 200	R	0.6	2.0	0.6	
200 – 100		0.5	2.8	0.5	
1000 – 850	C	2.2°	3.4°	0.7	
850 – 700	L	1.0	2.5	0.6	JAN 30
700 – 500	O	-1.1	1.8	0.8	–
500 – 400	U	-1.7	2.2	0.8	FEB 28
400 – 300	D	-2.0	2.9	0.5	(42)
300 – 200	(MW) Y	1.4	2.6	0.5	
200 – 100		0.0	2.1	0.5	
1000 – 850	C	3.0°	3.3°	1.0	
850 – 700	L	0.3	2.1	0.7	JUL 24
700 – 500	O	-0.1	2.1	0.6	–
500 – 400	U	-0.3	2.7	0.5	AUG 22
400 – 300	D	-0.5	3.4	0.4	(55)
300 – 200	(MW) Y	-0.5	2.1	0.7	
200 – 100		0.6	1.9	1.0	

Table 2
Sat-RAOB Comparison of Tropical Islands (29S-32N)

LAYER	RETR.	$\overline{SAT} - \overline{RS}$	RMS DIFF.	SAT. VAR. / RS. VAR.	DATES AND APPROX. PERCENTAGE
1000 – 850		-0.5°	1.0°	1.1	
850 – 700	C	0.4	0.8	1.0	JAN 30
700 – 500	L	0.2	0.9	1.0	–
500 – 400	E	0.7	1.1	1.0	FEB 28
400 – 300	A	1.0	1.9	0.7	(69)
300 – 200	R	0.5	1.6	0.6	
200 – 100		0.9	1.6	0.5	
1000 – 850		0.7°	1.3°	1.0	
850 – 700	C	0.9	1.7	0.8	JUL 24
700 – 500	L	0.4	1.5	0.7	–
500 – 400	E	0.1	1.7	0.8	AUG 22
400 – 300	A	-0.5	2.1	0.9	(77)
300 – 200	R	-0.4	1.5	0.6	
200 – 100		1.5	2.5	0.8	
1000 – 850	C	1.3°	2.6°	0.6	JAN 30
850 – 700	L	0.9	1.9	0.6	–
700 – 500	O	0.1	1.1	1.5	FEB 28
500 – 400	U	-1.0	1.5	1.4	(18)
400 – 300	D	-2.1	2.2	1.1	
300 – 200	(MW) Y	-0.5	2.6	1.1	(Very Few
200 – 100		3.6	3.9	1.4	Match-Ups)
1000 – 850	C	-1.2°	1.6°	0.9	
850 – 700	L	-1.0	1.9	0.6	JUL 24
700 – 500	O	-1.6	1.9	0.9	–
500 – 400	U	-2.4	2.8	1.3	AUG 22
400 – 300	D	-2.6	2.8	1.1	(10)
300 – 200	(MW) Y	-2.9	3.2	0.6	
200 – 100		0.2	1.2	1.8	

Table 3
Sat-RAOB Comparison of Seven to Eight Northern Hemisphere Ships and Islands (38–62N)

LAYER	RETR.	$\overline{SAT} - \overline{RS}$	RMS DIFF.	$\frac{SAT.\ VAR.}{RS.\ VAR.}$	DATES AND APPROX. PERCENTAGE
1000 – 850		-2.1°	2.9°	1.0	
850 – 700	C	0.7	2.1	0.7	JAN 30
700 – 500	L	1.3	2.6	0.6	–
500 – 400	E	0.9	2.5	0.6	FEB 28
400 – 300	A	0.6	2.2	0.8	(45)
300 – 200	R	-0.0	2.2	0.7	
200 – 100		-0.3	1.8	0.8	
1000 – 850		2.1°	2.8°	0.9	
850 – 700	C	0.4	1.6	0.8	JUL 24
700 – 500	L	-0.1	1.6	0.7	–
500 – 400	E	-0.1	1.9	0.6	AUG 22
400 – 300	A	-0.3	1.9	0.7	(69)
300 – 200	R	-0.2	1.6	0.5	
200 – 100		0.0	1.9	0.7	
1000 – 850	C	-2.1°	4.0°	1.2	
850 – 700	L	1.5	3.1	0.9	JAN 30
700 – 500	O	2.1	3.3	0.6	–
500 – 400	U	2.0	3.3	0.4	FEB 28
400 – 300	D	1.6	3.1	0.4	(45)
300 – 200	(MW) Y	1.3	2.8	0.8	
200 – 100		-0.3	1.6	0.9	
1000 – 850	C	4.4°	4.8°	0.7	
850 – 700	L	1.1	2.3	0.5	JUL 24
700 – 500	O	-0.0	1.6	0.5	–
500 – 400	U	-0.7	2.1	0.3	AUG 22
400 – 300	D	-1.2	2.1	0.4	(19)
300 – 200	(MW) Y	1.1	1.9	0.6	
200 – 100		0.2	2.0	0.4	

within retrieval schemes based upon regression. The NESS cloudy temperature retrievals below 100 mb use the following statistical predictors:

Channel	Peak Response	Remarks
MSU(1)	Surface	Affected by surface waves
MSU(2)	600 mb	
MSU(3)	290 mb	Off on NOAA-6 Christmas 1979 to July 1980
MSU(4)	90 mb	
HIRS(1)	30 mb	
HIRS(2)	60 mb	
HIRS(3)	100 mb	
HIRS(17)	2 mb	Little effect on sounding

(The four infrared channels are presumably not affected by tropospheric clouds and evidently carry some meaningful information about tropospheric temperature indirectly through the largely negative correlation between stratospheric and tropospheric temperatures in the atmosphere.)

The bias pattern on the bottom of Table 3 can be interpreted physically as follows:

1. Because of variable surface emissivity MSU(1) is not very useful over oceans. Temperatures below 600 mb and temperatures from 500 to 300 mb are, therefore, determined mostly by MSU(2) *plus the mean lapse rate of T below and above 600 mb found in the colocation base.*

2. In the belt 30-60N, the NESS colocation base is almost entirely (~90 percent) continental (and clear). Climatologically, the troposphere over continents in winter is more stable than that over the oceans and in summer is more unstable than over oceans. This produces the observed bias pattern.

3. NMC Maritime Colocation Program

A special maritime colocation program has been developed at NMC to test and correct this problem with current colocated RAOB data (Phillips *et al.*, 1979; Phillips, 1980). It uses a group of island stations (32-64N) and the five fixed ships (47-66N) in the Atlantic and Pacific. The sea-surface temperature obtained from the NMC sea-surface analysis is used as a ninth predictor in addition to brightness temperatures from the eight TOVS channels listed above. (For each of the

seven layers, only the best (and most reliable) of the nine predictors are used, usually about five.) Figures 1 and 2 compare the NMC and NESS results for TIROS-N last winter (51 days), while Figures 3 and 4 compare the NOAA-6 results for June 25 to July 7 (MSU3 missing).[1] The NESS bias results on Figures 1 and 3 are similar to the 1979 TIROS-N results on the bottom of Table 3. The NMC bias results are smaller and within the accepted $\sqrt{n}$ sampling error, and the temperature RMS errors are better than those for NESS.

An important use of satellite temperature retrievals in the NMC optimum analysis system is to use geopotential heights derived from those temperatures and a 1000-mb analysis to update the wind analysis in analysis volumes if little or no wind data is present. The geopotential differences from RAOBs produced by the NMC *microwave* scheme are only slightly larger than those produced by the NESS *infrared* retrievals.

4. Concluding Remarks

This NMC microwave retrieval method is being implemented now by NESS over the 30 to 65°N oceans. It is important because the NESS retrieval system produces 50 percent or more microwave retrievals over the extratropical oceans in winter. In the 1979 Northern Hemisphere summer, TIROS-N produced only 20 percent microwave retrievals over this area, but in 1980 (with NOAA-6) the fraction is now about 45 percent.

A smaller effort is now underway at NMC to consider use of satellite temperature retrievals over land. Canada, where RAOB stations are far apart, is of course the area of major interest. Table 4 shows a month of statistics for last winter in Canada, using both TIROS-N and NOAA-6. For the infrared retrievals, the bias and RMS error are similar to the oceanic values shown for February 1979 in Table 3. In the microwave case, the differences are smaller (except in the bottom layer) than those in Table 3.

The NESS retrieval system reports precipitable water (for the three layers, ground to 700 mb, 700 to 500, and 500 to 300) where infrared temperature retrievals can be made. We have found that:

a. In colocation collections of the size referred to in the above discussion of temperature retrievals, the bias in mean values of water vapor for the lowest layer is quite small.

b. The variance in the retrieval values, however, is only about 50 percent of that from the radiosondes. Analyses over the United States confirm this by showing a noticeable underestimate of large values.

We have not yet decided whether this moisture data will be useful in our analysis programs.

[1] NMC retrieval coefficients are based on colocations 1 to 2 weeks old.

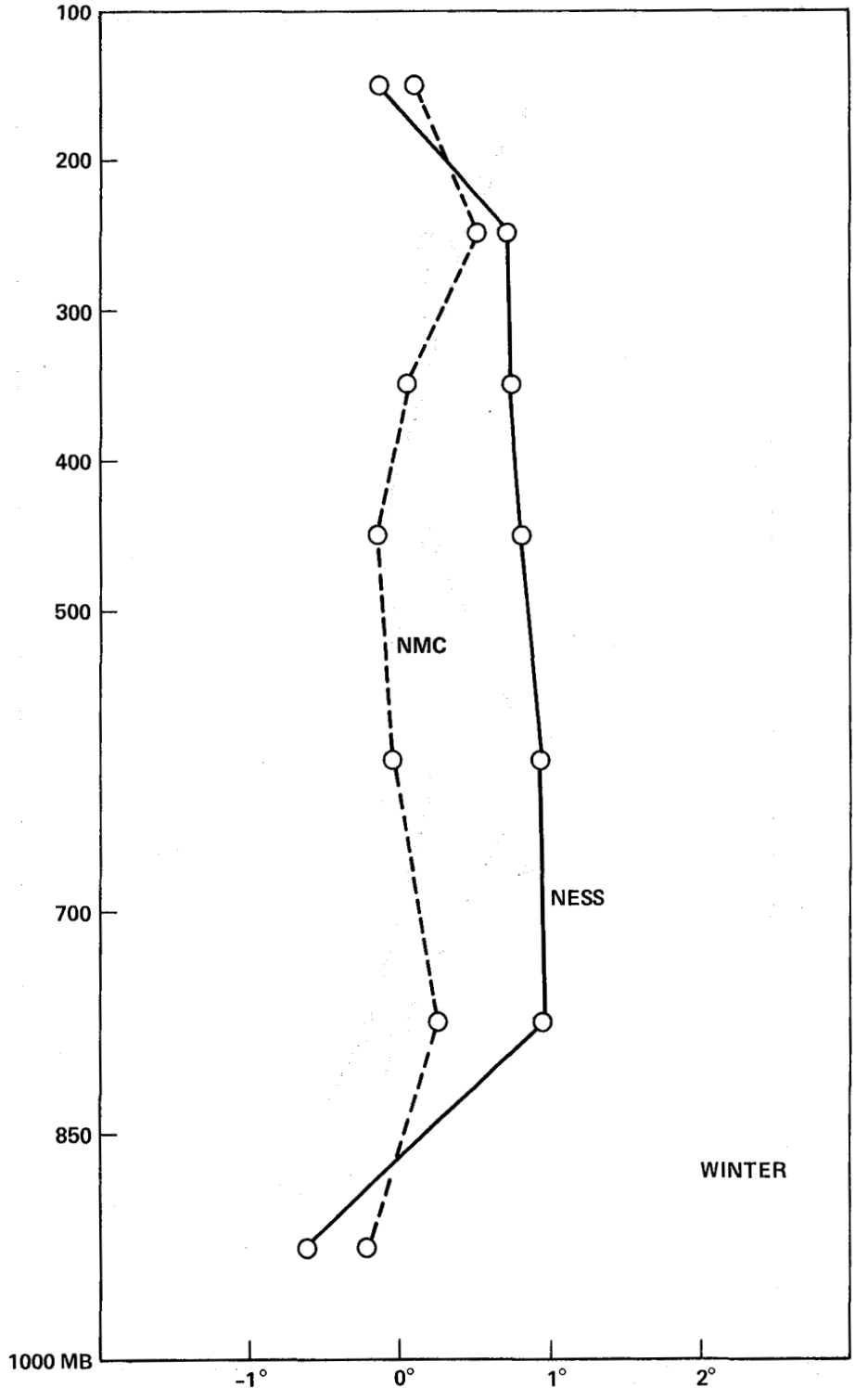

Figure 1. Bias, 3rd path TIROS-N, Dec. 1, 1979 – Jan. 20, 1980, Atlantic-Pacific 32-66°N (Sat-RAOB).

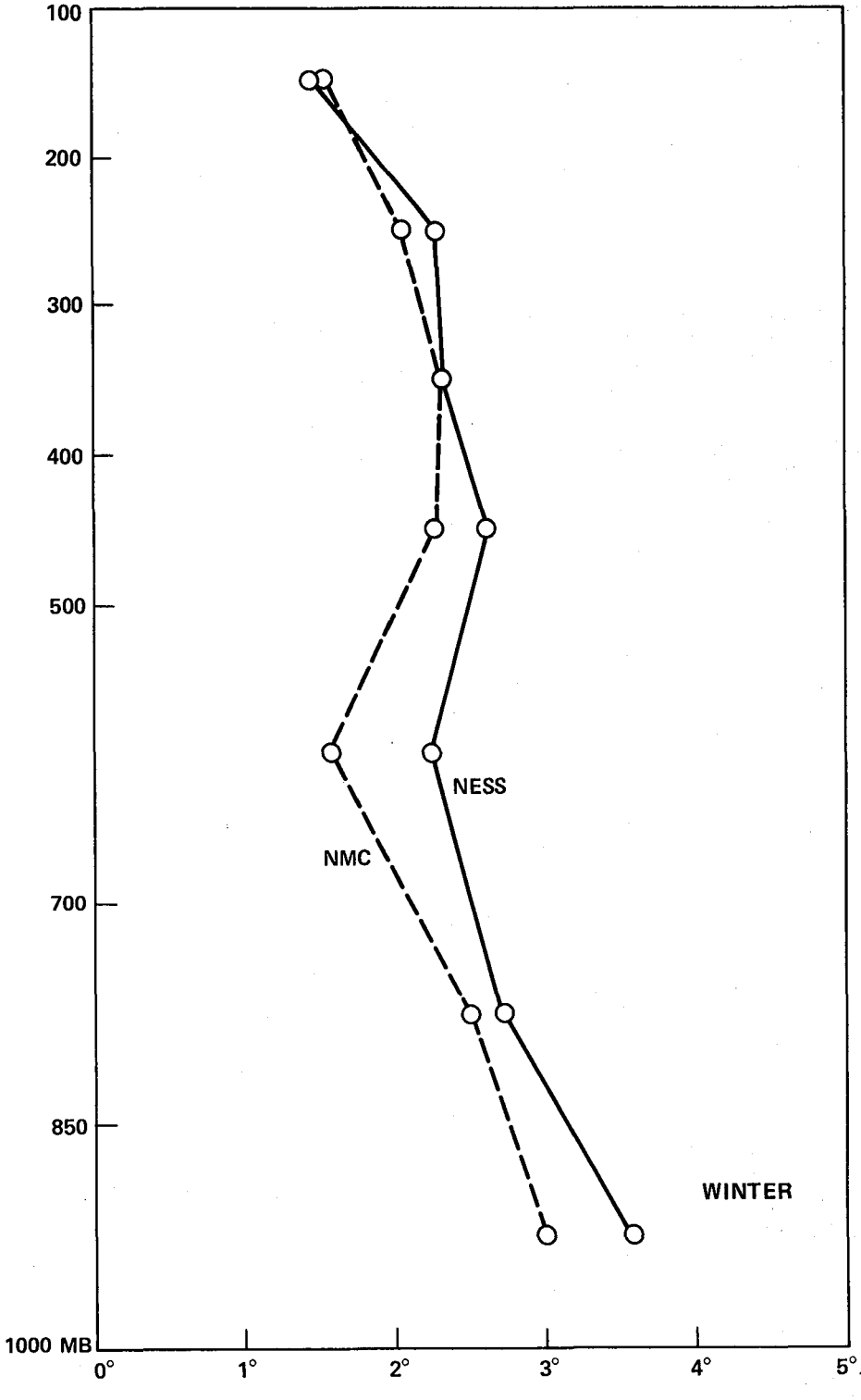

Figure 2. RMS, 3rd path TIROS-N, Dec. 1, 1979 – Jan. 20, 1980, Atlantic-Pacific 32-66°N

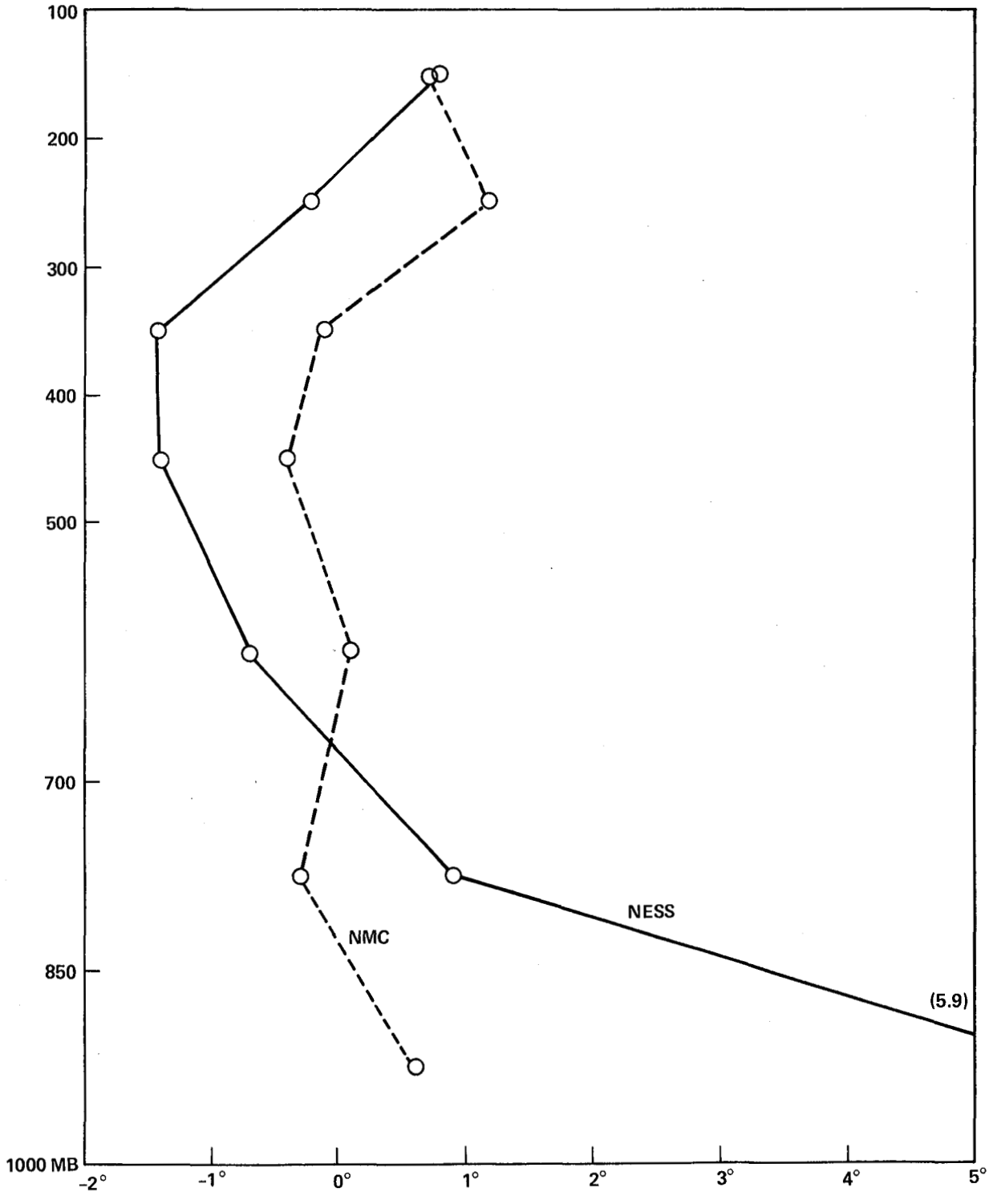

Figure 3. Bias (Sat–RAOB) 3rd path NOAA-6, June 25 – July 7, 1980, Atlantic-Pacific 32–66°N.

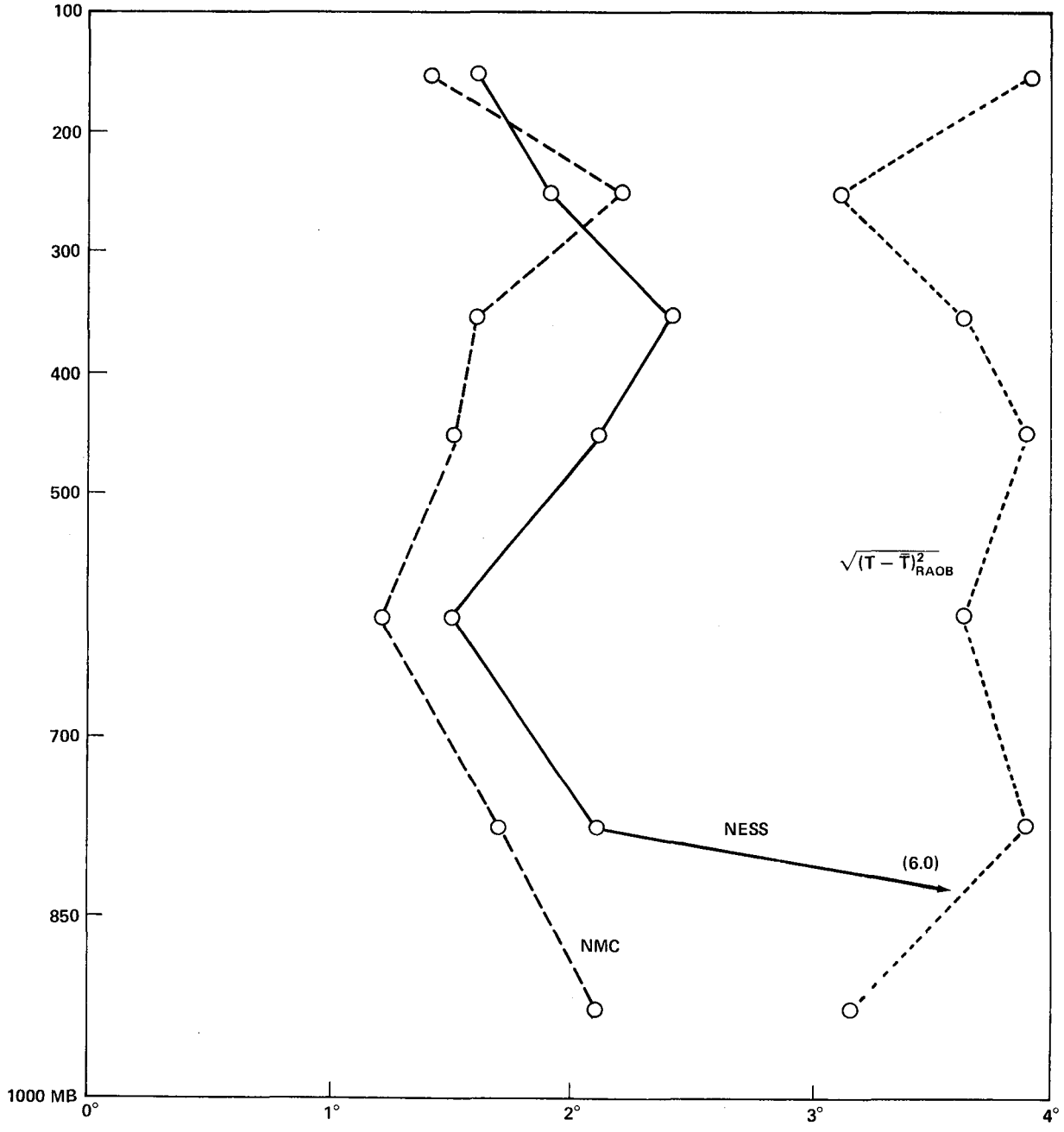

Figure 4. RMS (Sat-RAOB) 3rd path NOAA-6, June 25 – July 7, 1980, Atlantic-Pacific 32-66°N.

Table 4
Sat-RAOB Comparison of Nine Canadian Stations (46-74N) for Nov. 13 to Dec. 15, 1979
as Derived from TIROS-N and NOAA-6

LAYER		$\overline{SAT} - \overline{RS}$	RMS DIFF.	SAT. VAR. / RS. VAR.
1000 – 850		0.6	2.7	1.1
850 – 700	C	-0.6	2.2	1.0
700 – 500	L (~200)	0.7	1.9	0.8
500 – 400	E	1.2	2.6	0.7
400 – 300	A	1.0	2.3	0.8
300 – 200	R	0.1	1.9	0.7
200 – 100		0.4	1.6	0.8
1000 – 850	C	2.6	5.2	1.8
850 – 700	L (~150)	-0.2	3.0	0.8
700 – 500	O	0.0	2.2	0.8
500 – 400	U	-0.1	2.6	0.7
400 – 300	D	0.1	3.1	0.7
300 – 200	Y	-0.1	2.1	1.0
200 – 100		0.9	1.7	0.8

Microwave radiances are affected by the larger water drops, such as are found in precipitation. The result is usually a tropospheric temperature retrieval that is too cold, much as would result from ignoring any clouds present in an infrared retrieval. Together with NESS, we have instituted a simple test to recognize those microwave temperature retrievals *over the ocean* that are affected by precipitation (see Ref. 3). The brightness temperature from MSU1 over the ocean is typically 20 to 30 degrees less than that from MSU2 because of the low surface emissivity of the sea. Precipitation warms MSU1 and (slightly) cools MSU2. We have found that

$$(\text{MSU2} - \text{MSU1}) < 12^\circ$$

indicates precipitation significant enough that the tropospheric retrieval temperatures should be discarded. NESS has used this test since February 1980. If VAS includes microwaves, an equivalent test would be necessary over land.

References

1. Phillips, McMillin, Gruber and Wark, 1979: An evaluation of early operational temperature soundings from TIROS-N. *Bull. Amer. Meteor. Soc., 60,* 1188-1197.

2. Phillips and Desmarais, 1979: The use of TIROS-N temperature data in the NMC analysis-forecast models. *Preprint Vol. of Fourth Conf. on Numerical Weather Prediction, 1979.* Amer. Meteor. Soc., Boston (pp. 340-344).

3. Phillips, N., 1980: Two examples of satellite temperature retrieval in the North Pacific. *Bull. Amer. Meteor. Soc.* (To appear in vol. 61, July).

4. Phillips, N., 1980: Cloudy winter satellite temperature retrievals over the extratropical Northern Hemisphere Ocean. (Submitted to *Mon. Wea. Rev.)*

EVALUATION OF NESS SOUNDINGS USED IN THE FGGE SPECIAL EFFORT

Robert Atlas
Laboratory for Atmospheric Sciences
NASA/Goddard Space Flight Center

1. Introduction

The FGGE Special Effort is being conducted for the two FGGE special observing periods (January to March and May to June 1978) as a joint project between NASA, NOAA, and the University of Wisconsin. Man-computer Interactive Data Access System (McIDAS) terminals developed by the Space Science Engineering Center (SSEC) of the University of Wisconsin are being utilized by experienced meteorologists at the National Meteorological Center (NMC) for data evaluation and quality assessment and at the Goddard Laboratory for Atmospheric Sciences (GLAS) for satellite data enhancement. The interactive procedures used for sounding and cloud-motion wind enhancement were originally developed by the National Environmental Satellite Service and SSEC. (Smith *et al.*, 1978, and Menzel *et al.*, 1978). (See Greaves *et al.*, 1979 for a detailed description of the development and implementation of the FGGE Special Effort.)

For each synoptic period there is an initial editing of FGGE data by NMC. At this stage, quality indicators are assigned to temperature soundings from TIROS-N and to cloud-tracked wind vectors from geostationary satellites. The determination of data quality is made on the basis of synoptic considerations, including horizontal, vertical and temporal consistency. Regions where data deficiencies exist or where higher resolution data is needed to adequately represent the atmospheric thermal structure are then selected for enhancement. The eastern North Pacific is routinely enhanced because of the importance of this region to forecasting for North America. In addition, more than 60 cases have been selected for enhancement, on the basis of meteorological interest, by an *ad-hoc* international committee of participating scientists. These cases include situations of blocking, cut-off low development, cyclogenesis, and tropical circulation.

The sounding data enhancement is aimed at supplementing the operational satellite sounding data set with higher resolution soundings in meteorologically active regions and with new soundings where data voids or soundings of questionable quality exist. The algorithms for retrieving temperature profiles from the TIROS-N observations of radiance displayed on McIDAS are essentially the same as those used by NESS for the objective generation of operational temperature profiles. Three types of temperature retrievals are possible: (1) clear-column and (2) partly cloudy retrievals utilizing infrared observations from the HIRS instrument aboard TIROS-N, and (3) cloudy retrievals utilizing only microwave observations from the Microwave Sounding Unit (MSU) on TIROS-N. The operational temperature profiles have a horizontal resolution of 250 km, whereas special effort temperature profiles can be retrieved at the resolution of the measurements (30 km for HIRS and 150 km for MSU).

The sounding enhancement process at GLAS is performed as follows: once an area has been selected, the McIDAS operator begins by displaying all available conventional and special FGGE data for that area and visible, infrared, and microwave images from TIROS-N. The operator notes where data deficiences exist and, from the TIROS-N images, determines the extent of cloudiness and where the most intense atmospheric thermal gradients are located. High-resolution infrared temperature retrievals are then generated for the area. This is followed by a comprehensive manual editing of the retrievals to remove small-scale discontinuities due to cloud-induced noise while retaining significant meteorological structures. Enhanced microwave retrievals, consistent with neighboring infrared retrievals, are then generated in cloudy areas.

After the entire enhancement process is completed, a final editing and quality assessment of the enhanced data is performed at NMC. The data is then archived as supplementary Level IIb and will be utilized by NOAA's Geophysical Fluid Dynamics Laboratory (GFDL) in generating Level IIIb analyses.

2. Results

At the present time, only a limited number of enhancements have been performed and the applications of Special Effort data to weather analysis and forecasting are just beginning. Enhanced sounding data can be displayed on the McIDAS as either mandatory level temperatures or as the thickness between any two levels. Analyses of these quantities as well as thermal winds, vertical temperature profiles, and vertical cross-sections of potential temperature are routinely produced. If conventional surface data is available, then the 1000-mb geopotential height is analyzed, and the satellite-derived thickness and thermal winds are added to the 1000-mb height and 1000-mb geostrophic wind to yield geopotential height and geostrophic winds on constant pressure surfaces. In addition to the high resolution analyses performed directly on the McIDAS, enhanced soundings may be assimilated into larger scale objective analyses which then serve as initial conditions for numerical model predictions.

Subjective comparisons of enhanced soundings with all available operational soundings and radiosonde reports are performed at the end of the enhancement process. These comparisons have shown that the enhanced and operational retrievals tend to be similar in cloud-free areas. However, large differences occasionally occur. The differences are accentuated in and around cloudy areas where the interactive processing at high resolution allows for the generation of substantially more infrared retrievals and where the microwave retrievals are enhanced.

Examples illustrating some of the effects of the sounding data enhancement are presented in Figures 1 and 2. In Figure 1, 1000- to 300-mb thickness analyses of operational (solid lines) and Special Effort retrievals (dashed lines) and plotted radiosonde reports are shown for a section of the North Pacific at 0100 GMT 7 January 1979. Large differences in the orientation, gradient, and absolute value of the enhanced and operational thickness contours are evident. In addition, the errors relative to colocated radiosondes have been reduced by 30 to 80 geopotential meters.

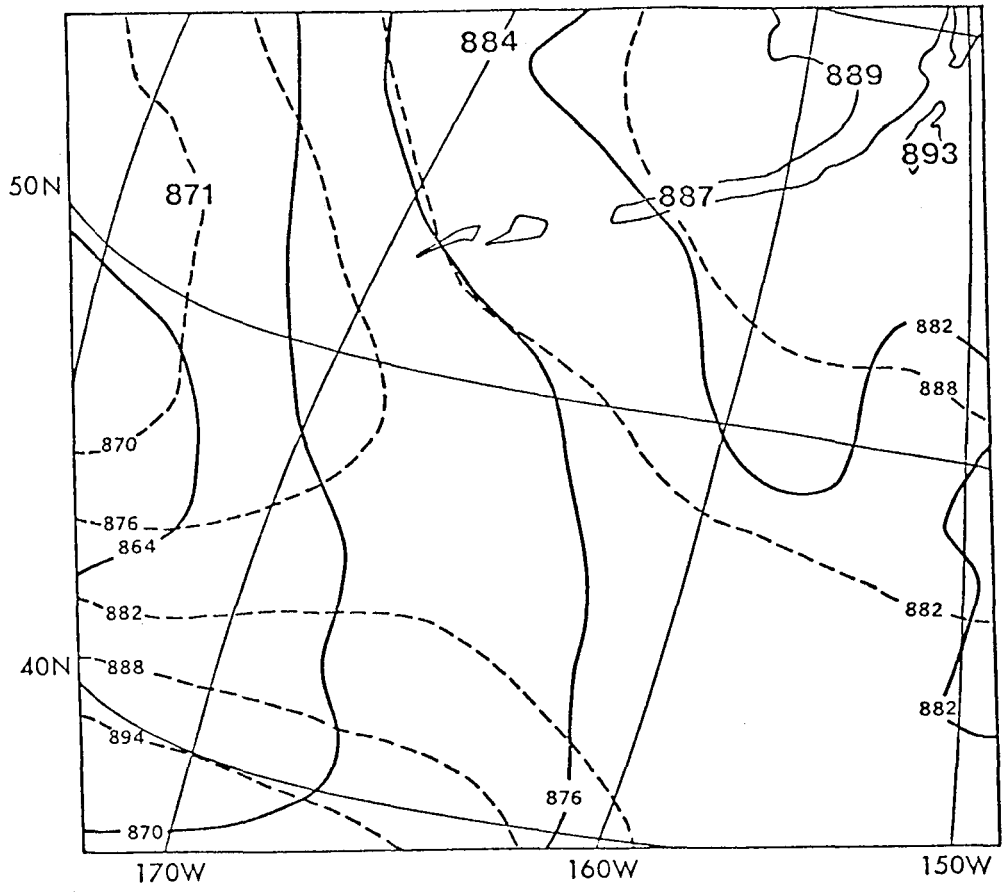

Figure 1. 1000-300 mb thickness analyses of operational soundings (solid lines) and Special Effort soundings (dashed lines) for 0100 GMT 7 Jan 79. Radiosonde observations of 1000-300 mb thickness in decameters are plotted as large numbers.

In Figure 2, vertical temperature profiles of unenhanced and enhanced microwave retrievals are plotted relative to the colocated radiosonde observation at Yakutat, Alaska at 0000 GMT 11 January 1979. Differences between the retrievals are small throughout most of the troposphere in this case. However, the enhancement process has resulted in a better definition of the tropopause and a reduction of error of 4°C near the 100-mb level.

As an example of the application of Special Effort sounding to large-scale meteorological analysis and prediction, the enhancement for 0000 GMT 9 January 1979 is presented here. This was a case in which a large gap in the operational TIROS-N soundings occurred in the eastern North Pacific. Figure 3 shows the orbit of TIROS-N and the location of operational soundings from 2100 GMT 8 January to 0300 GMT 9 January. Reprocessing of observed radiances on the McIDAS allowed for the generation of enhanced soundings over a large portion of the data gap from 30 to 50°N. Additional high resolution soundings were also generated over regions adjacent to the gap to better define the atmospheric thermal structure and to insure consistency.

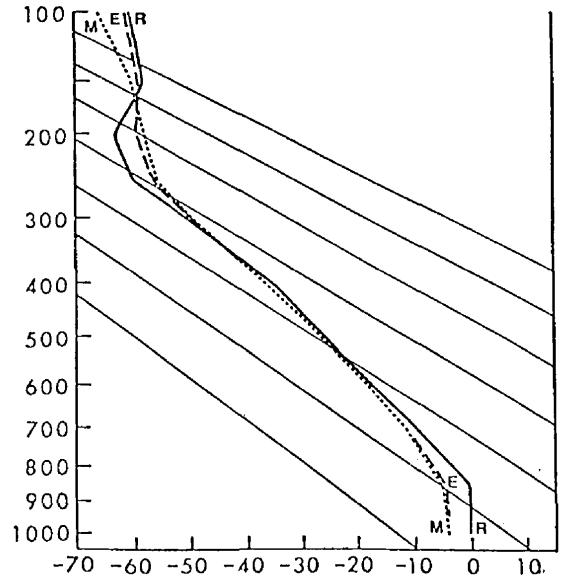

Figure 2. Vertical temperature profiles derived from unenhanced microwave (M), enhanced microwave (E), and radiosonde (R) for Yakutat, Alaska, at 0000 GMT 11 Jan 79.

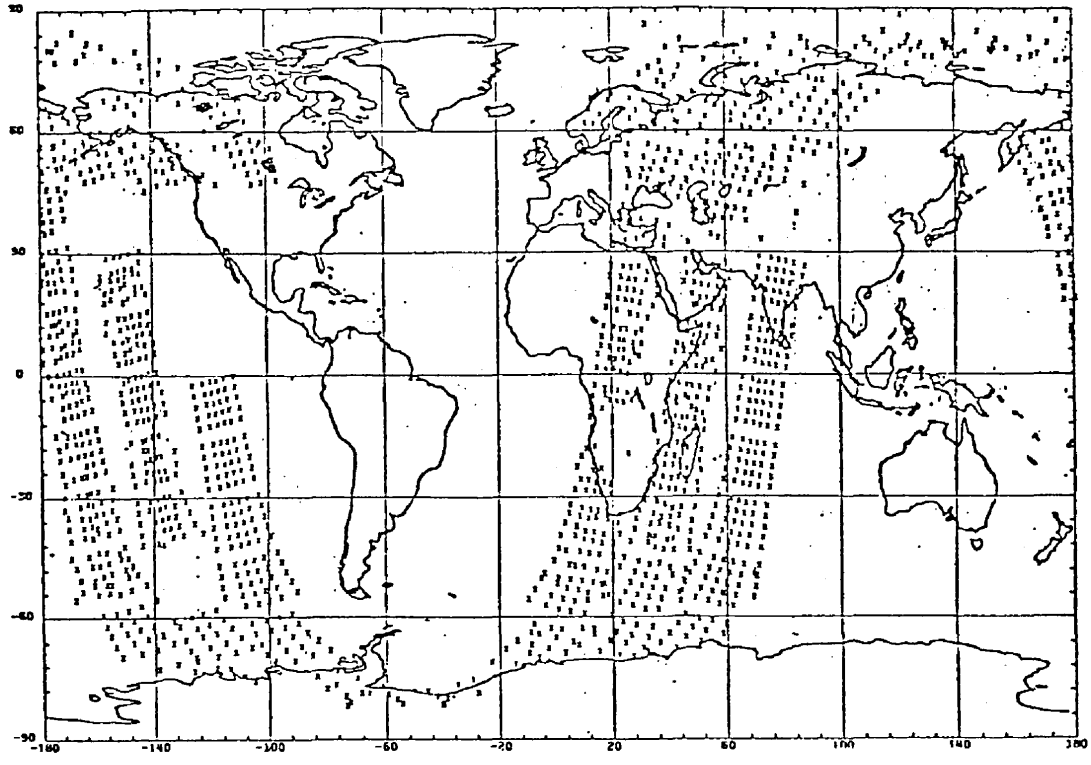

Figure 3. Location of TIROS-N retrievals from 2100 GMT 8 Jan 79 – 0300 9 Jan 79.

Figures 4 and 5 display the 1000 to 300-mb thickness analyses and thermal winds for the enhanced regions. These analyses are based completely on the high-resolution soundings, with each thermal wind barb plotted at the location of the retrieved vertical temperature profiles.

Figures 6 and 7 illustrate the effect of the enhanced soundings on the GLAS objective analysis for 0000 GMT 9 January. In Figure 6, the 300-mb height and wind analysis for all conventional and operational satellite data is presented. The corresponding analysis, which includes enhanced soundings, is presented in Figure 7. Comparison of the figures reveals that a major modification to 300-mb heights and winds has occurred just off the West Coast of the United States. The enhanced soundings have increased the amplitude of the ridge at 135 W and shortened the half-wavelength between this ridge and the trough along the West Coast. Elsewhere the effects are smaller due to the consistency of the operational and enhanced soundings over most of the eastern North Pacific and the averaging of the effects of the enhanced soundings by the objective analysis. However changes to the intensity of the geopotential gradient and orientation of the winds and contours are evident throughout this region.

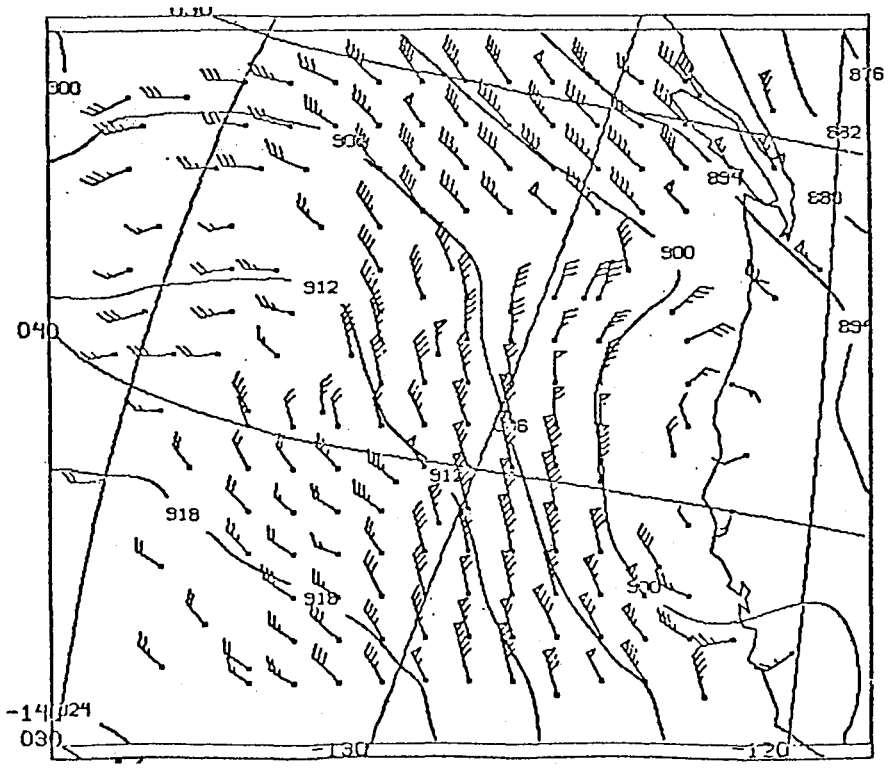

Figure 4. 1000-300 mb thickness and thermal wind at 2300 GMT 8 Jan 79 derived from high resolution TIROS-N soundings for the region 30-55°N and 120-145°W.

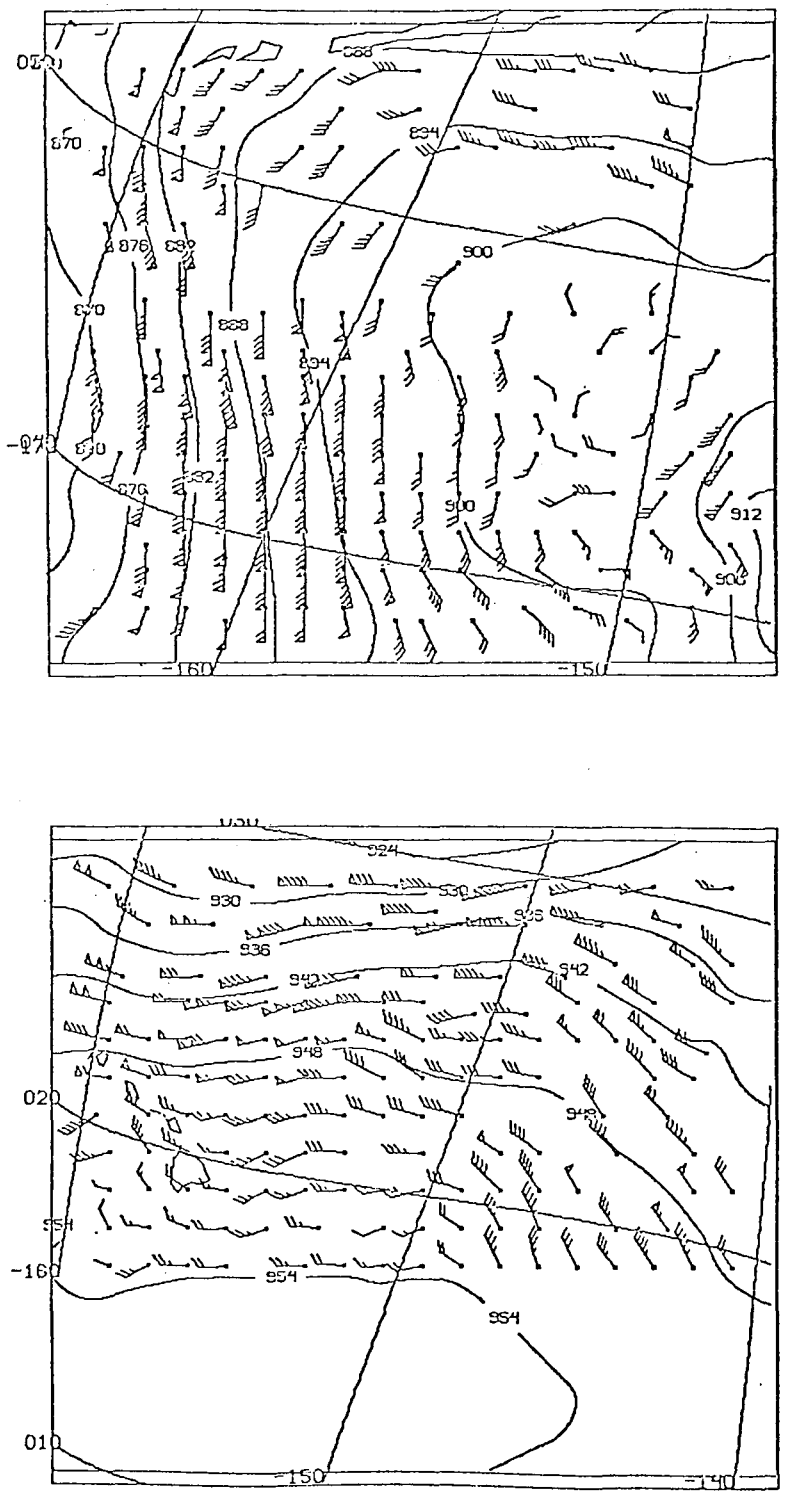

Figure 5. 1000-300 mb thickness and thermal winds at 0100 GMT 9 Jan 79 derived from high resolution TIROS-N soundings for the region 10-60°N and 140-170°W.

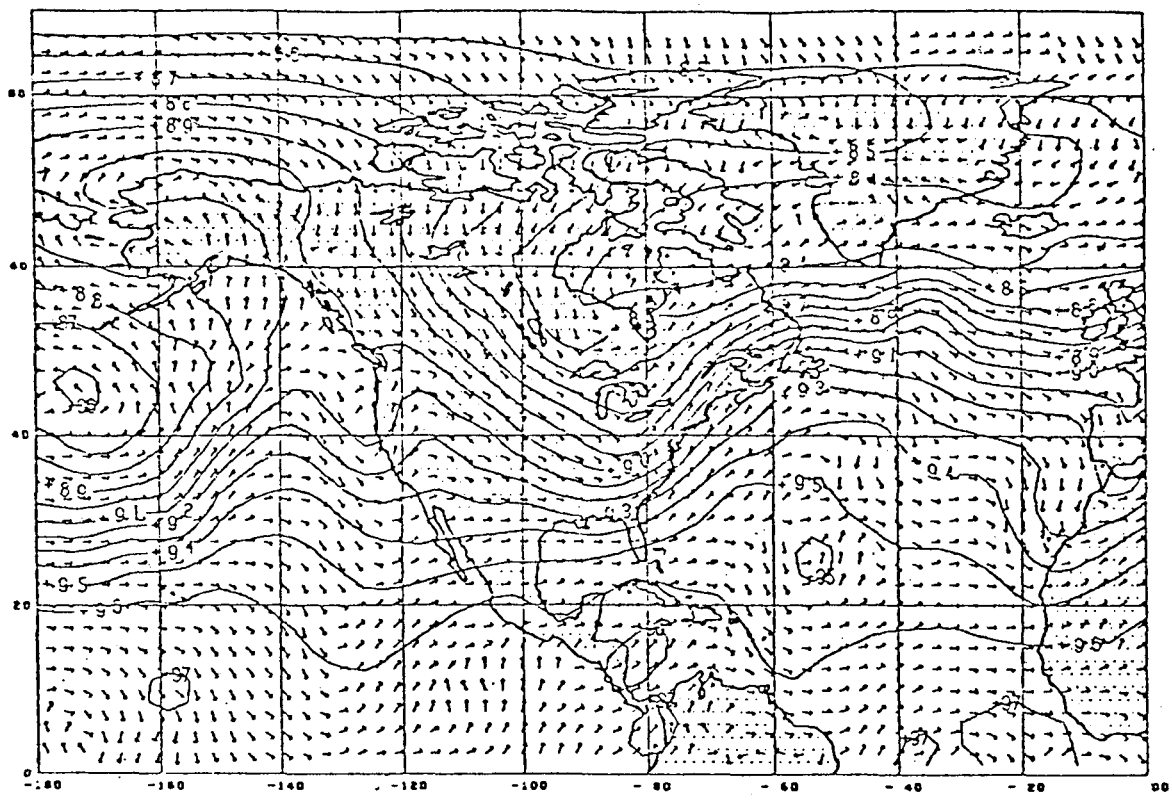

Figure 6. 300 mb geopotential height and wind analysis without enhanced retrievals for 0000 GMT 9 Jan 79.

Figures 8 and 9 show the 24-hour GLAS model forecasts of 300-mb geopotential heights and winds, which were generated from initial conditions corresponding to Figures 6 and 7, respectively. The verifying analysis is presented in Figure 10. Comparison of these figures reveals that the inclusion of enhanced soundings resulted in a large improvement in the predicted amplitude of the trough over the southwestern United States. Additional improvements are evident over the North Pacific. However, the verifying analysis is less certain in this area.

4. Summary

A special effort to produce high-quality edited and enhanced global data sets is being conducted for the two special observing periods of FGGE. More than 60 cases have been selected for enhancement on the basis of meteorological interest. These cases include situations of blocking, cut-off low development, cyclogenesis, and tropical circulations. The sounding data enhancement process consists of supplementing the operational satellite sounding data set with higher resolution soundings in meteorologically active regions and with new soundings where data voids or soundings

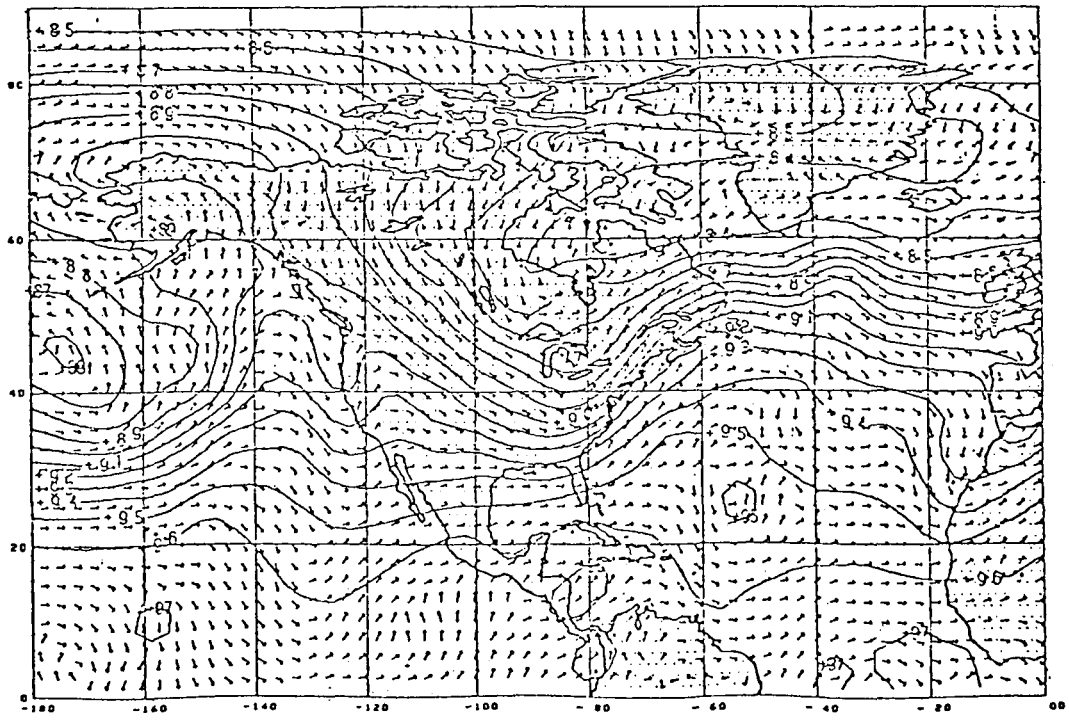

Figure 7. 300 mb geopotential height and wind analysis with enhanced retrievals for 0000 GMT 9 Jan 79.

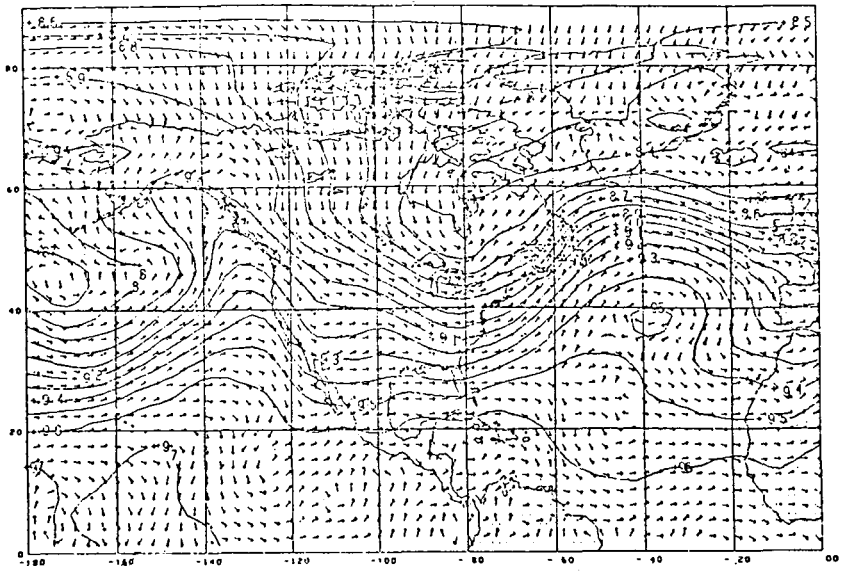

Figure 8. 24h 300 mb forecast generated without enhanced retrievals.

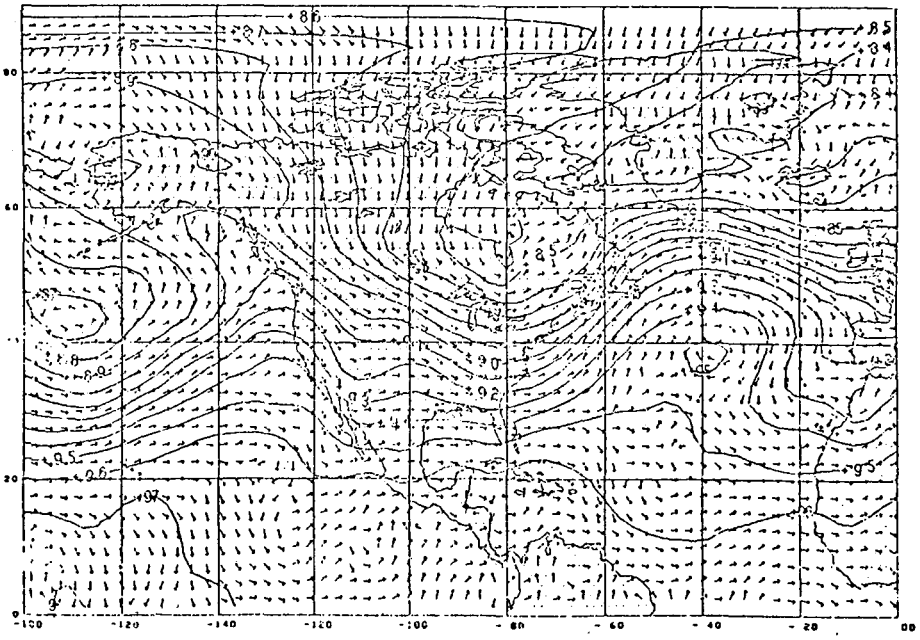

Figure 9. 24h 300 mb forecast generated with enhanced retrievals.

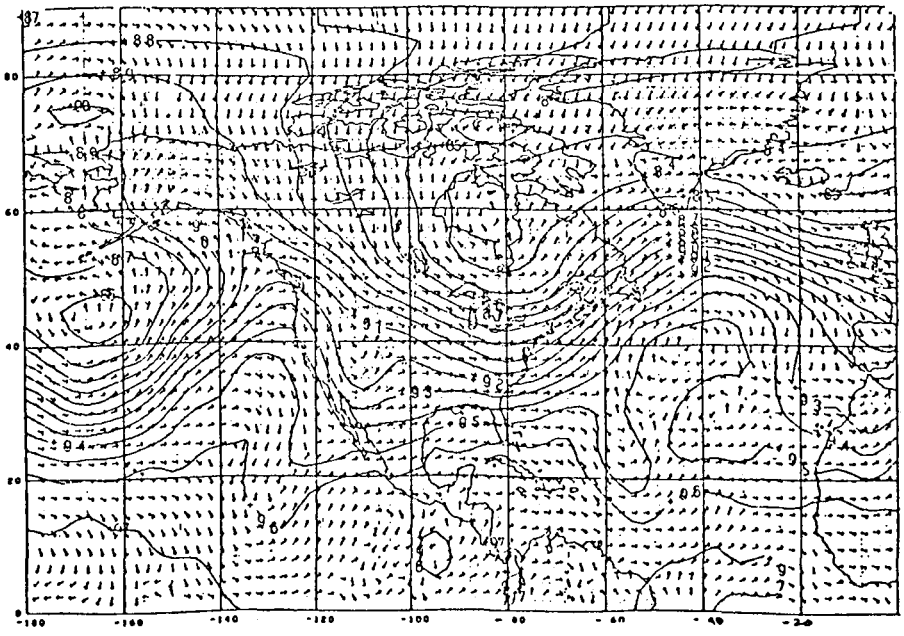

Figure 10. Verifying 300 mb geopotential height and wind analysis for 0000 GMT 10 Jan 79.

of questionable quality exist. After the enhancement process is completed, a final editing and quality assessment of the enhanced data are performed. The data is archived as supplementary level IIb and will be utilized in level IIIb analyses.

Subjective evaluation of the effects of sounding data enhancement indicate that:

1. Enhanced and operational IR retrievals are similar in most situations.

2. Large improvements in 1000 to 300-mb thickness and mandatory level temperature and intensification of atmospheric thermal gradients occasionally occur.

3. Interactive processing can fill in major gaps in the TIROS-N coverage.

4. Assimilation of Special Effort soundings can result in major modifications to large-scale analyses and prognoses.

Acknowledgment

The author wishes to acknowledge G. Cole, R. Rosenberg, and A. Pursch of the Special Effort Data Enhancement Team, and D. Edelmann, D. Sakal, M. Iredell, D. Wallace, and G. Chatters for their respective roles in implementing the McIDAS system at GLAS.

References

1. Greaves, J. R., G. DiMego, W. L. Smith, and V. E. Suomi, 1979: A special effort to provide improved sounding and cloud motion wind data for FGGE. *Bull. Amer. Meteor. Soc., 60,* 124-127.

2. Menzel, W. P., W. L. Smith, and H. M. Woolf, 1978: A man interactive technique for specifying cloud height from sounding radiance data. *Proc. of the Third AMS Conf. on Atmos. Rad.*, Davis California, 28-30 June.

3. Smith, W. L., C. M. Hayden, H. M. Woolf, H. B. Howell, and F. W. Nagle, 1978: Interactive processing of TIROS-N sounding data. *Proc. of the AMS Conf. on Wea. Forecasting and Analysis and Aviation Meteor.*, Silver Spring, Maryland, 16-19 October.

THE GLAS PHYSICAL INVERSION METHOD FOR ANALYSIS OF TIROS-N DATA

Joel Susskind
Laboratory for Atmospheric Sciences
NASA/Goddard Space Flight Center

Joan Rosenfield
Sigma Data Services Corporation
Silver Spring, Maryland

1. Introduction

Temperature sounding data from the TIROS-N/NOAA-6 complex of HIRS2, MSU, and SSU instruments is analyzed operationally by NOAA/NESS using statistical regression techniques. These techniques utilize statistical relationships between satellite-observed brightness temperatures and atmospheric temperature profiles to determine the temperature profile from the satellite radiance measurements. The regression relationships are obtained by simultaneous analysis of satellite-observed brightness temperatures and colocated radiosonde reports, using a data base from a previous time period.

The strength of the method lies primarily in relative simplicity in that there is no need to solve the atmospheric radiative transfer equations at all, let alone with a high degree of accuracy. The method has some weaknesses, however, foremost among which is the significant dependence of observed brightness temperature on other factors besides the temperature profile. These factors include the satellite zenith angle of observation, the humidity and ozone profile, the surface elevation, temperature, emissivity, and reflectivity, the effects of atmospheric liquid water on microwave observations, and, most significant of all, the effects of clouds on the infrared observations. Regardless of the method of analysis, these factors must be sufficiently accounted for or significant errors will occur in the retrieved temperature profiles. Moreover, it is desirable to have a way of determining if a problem exists in accounting for these effects. Another shortcoming of a statistical regression analysis scheme is the dependence on the applicability of a statistical ensemble to the case under study. Problems may arise in cases of synoptic situations or even whole geographic areas not well represented in the sample.

The GLAS approach to temperature sounding from satellite observations is fundamentally different from that of NESS in that heavy reliance is placed on the ability to model accurately the instrumental response to atmospheric and surface conditions, while no use is made of statistical relationships between satellite observations and atmospheric temperature profiles. The method involves starting with a guess set of atmospheric and surface conditions from which expected brightness temperatures for the satellite observations are computed. Then, iterative relaxation of atmospheric and surface conditions is performed according to the difference between observed and computed brightness temperatures until sufficient agreement is reached. In the absence of sufficient agreement, no retrieval is produced for that location.

The GLAS iterative scheme, based on the method of Chahine (1970, 1974), is comprised sequentially of the following elements:

1. Computation of clear-column radiances from a set of initial conditions.

2. Determination of iterative reconstructed clear-column radiances from potentially cloud-contaminated radiances.

3. Determination of the iterative ground temperature.

4. Recalculation of clear-column radiances using the iterative ground temperature.

5. Comparison of iterative reconstructed and calculated clear-column radiances.

6. If sufficient agreement is not found in step 5, calculation of the next (iterative) temperature profile and its clear-column radiances and a return to step 2.

The computation of clear-column radiances is done using rapid algorithms dependent on the temperature – humidity profile, zenith angle of observation, and surface temperature, emissivity, and pressure. The details of the transmittance algorithm dependence on temperature profile, water vapor profile, and zenith angle of observations, will not be discussed here. The following sections will describe:

1. The forward problem.

2. The relaxation equations for determining the atmospheric temperature profile.

3. The method of accounting for effects of clouds on infrared radiances.

4. The procedure for retrieval of sea or land surface temperature and accounting for solar radiation effects. The last section will compare the quality of the NESS and GLAS retrievals of HIRS/MSU data for Jan/Feb 1979.

2. The Radiative Transfer Equation "The Forward Problem"

Given atmospheric and surface conditions, the clear-column radiances R_i observed by a sounding channel i can be expressed as

$$R_i = \epsilon_i B_i[T_s]\, \tau_i(P_s) + (1 - \epsilon_i)\, R_i \downarrow\, \tau_i(P_s) + \rho_i' H_i \tau_{is}(P_s) + \int_{\ln P_s}^{\ln \bar{P}} B_i[T(P)]\, \frac{d\tau_i}{d \ln P}\, d \ln P \qquad (1)$$

where ϵ_i is the surface emissivity averaged over sounding channel i, $B_i[T]$ is the mean Plank black-body function, averaged over channel i, of the temperature T, $\tau_i(P)$ is the mean atmospheric transmittance from pressure P to the top of the atmosphere and evaluated at θ, the zenith angle of the observation, $R_i\downarrow$ is an effective atmospheric emission downward flux, $\rho_i' H_i \tau_{is}(P_s)$ is the reflected solar radiation in the direction of the satellite, and the subscript s refers to surface. The integral, taken from the surface to the satellite pressure $\overline{P}$, represents the upwelling atmospheric-emitted radiation, which is a mean value of the black-body function of atmospheric temperature weighted by the channel weighting function $d\tau_i/d\ln P$. Table 1 shows the channels, centers, and peak of the weighting functions, or other relevant information, for the channels on MSU and HIRS. The current analysis does not employ the SSU observations. The HIRS and MSU channels used in the analysis are designated by *.

Table 1
HIRS2 and MSU Channels

Channel	$\nu(cm^{-1})$	Peak of $d\tau/d\ln p$ (mb)	Peak of $Bd\tau/d\ln p$ (mb)
H1	668.40	30	20
*H2	679.20	60	50
H3	691.10	100	100
*H4	703.60	280	360
H5	716.10	475	575
H6	732.40	725	875
H7	748.30	Surface	Surface
H8	897.70	Window, sensitive to water vapor	
H9	1027.90	Window, sensitive to O_3	
H10	1217.10	Lower tropospheric water vapor	
H11	1363.70	Middle tropospheric water vapor	
H12	1484.40	Upper tropospheric water vapor	
*H13	2190.40	Surface	Surface
*H14	2212.60	650	Surface
*H15	2240.10	340	675
H16	2276.30	170	425
H17	2310.70	15	2
*H18	2512.00	Window, sensitive to solar radiation	
*H19	2671.80	Window, sensitive to solar radiation	
*M1	50.30[a]	Window, sensitive to surface emissivity	
*M2	53.74[a]	500	
*M3	54.96[a]	300	
*M4	57.95[a]	70	

[a]Values in GHz.

The transmittance functions for the HIRS channels are taken to be a product of dry transmittance functions, parameterized as a function of temperature profile and zenith angle, [Mo and Susskind, 1978] and effective water vapor transmittances of the form

$$\tau_i(P, \theta) = e^{-a_i W (P/P_s)^{n_i}}$$

where W is the column density of water vapor and a_i and n_i are channel-dependent constants [Susskind *et al.*, 1977]. The infrared emissivity ϵ_i is taken as 0.95 or 0.98 for land and water, respectively, at wavelengths greater than 10 μm, and 0.85 or 0.95 for wavelengths less than 5 μm (channels between 5 μm and 10 μm were not used in the analysis). The effective downward flux, $R_i\downarrow$, is calculated according to Kornfield and Susskind [1977]. The solar radiation term is discussed in the section dealing with retrieval of surface temperature.

The microwave transmittances are taken to be products of O_2 transmittances, calculated as a function of temperature profile and zenith angle according to Rosenkrantz [1975], and water vapor transmittances having the same form as the infrared effective water vapor transmittances. Water vapor retrievals using the humidity sounding channels on HIRS2 are not done at this time, and W, the water vapor column density, is estimated at the 24-hour-lag analysis value, as is the surface pressure P_s. The microwave emissivity is calculated from the 50.3 GHz channel, as part of the iterative scheme, according to

$$\epsilon = \frac{R_i - \int T d\tau - R_i\downarrow \tau_i(P_s)}{[T_s - R_i\downarrow]\, \tau_i(P_s)} \qquad (2)$$

where R_i is the 50.3 GHz observed brightness temperature, T_s is the iterative surface temperature, and T(P) is the iterative atmospheric temperature profile used in the calculation of the upward and downward microwave fluxes emitted by the atmosphere. The transmittance functions are corrected for temperature, water vapor, and zenith angle as described earlier, but possible effects of liquid water attenuation on the 50.3 GHz channel are not accounted for. The emissivity determined from the 50.3 GHz channel observation is used, together with the iterative temperature profile, to calculate brightness temperatures for the other MSU channels.

The effects of clouds on infrared radiances is not treated explicitly. On the other hand, a set of reconstructed clear-column radiances, that is estimations of radiances which would have been observed if the field of view were completely clear, is produced for each infrared channel in a manner to be described later.

3. The Atmospheric Temperature Profile Relaxation Equation

The relaxation method of finding a solution to a set of radiative transfer equations was developed by Chahine (1970). It differs from other methods in that it does not attempt, in any iteration,

to find a best solution to the set of equations (observations) but only to provide a set of parameters giving better agreement of observed and calculated radiances than obtained in the previous iteration. The iterative method is computationally faster than methods to solve the inverse radiative transfer directly and is also more stable. Moreover, to solve the inverse radiative transfer equation, it is necessary first to put the equation in approximate linear form with coefficients which are profile-dependent. Therefore, an "exact" solution must be iterative in any event.

In the iterative relaxation scheme, modifications to the temperature profile are made according to the difference of observed and computed radiances in temperature sounding channels weighted by the sensitivity of observations in these channels to changes in temperature in different parts of the atmosphere. Before comparisons of Nth iterative observed and calculated radiances can be made, one must first modify the observations to give reconstructed clear-column radiances $\hat{R}_i^N$ and also determine everything necessary to compute radiances R_i^N for a given temperature profile, $T^N(P)$ from equation 1. Given $\hat{R}_i^N$ and R_i^N, it is most convenient to compare the observed and computed brightness temperatures, $\hat{T}_i^N$ and T_i^N, because of an essentially linear relationship between changes in brightness temperature with changes in temperature profile. These brightness temperatures are defined as the inverse black-body function of the radiances evaluated at the mean channel frequency ν_i.

From equation 1, we see that to a good approximation, brightness temperatures for two closely related temperature profiles T(P) and T(P) + δ(P), will differ by

$$T_i[T(P) + \delta(P)] - T_i[T(P)] = \int W_i(P)\, \delta(P)\, d\ln(P) \tag{3}$$

where

$$\begin{aligned} W_i(P) &= \left[\frac{dT_i}{dR_i}\right]_{R_i} \left[\frac{dR_i}{dT}\right]_{T(P)} \\ &= \left[\frac{dT}{dB_i}\right]_{T_i} \left[\frac{dB_i}{dT}\right]_{T(P)} \left[\frac{d\tau_i}{d\ln P}\right]_{P} \end{aligned} \tag{4}$$

assuming all else remains constant. Figure 1 shows the weighting functions as defined in equation 4, relating the change in brightness temperature to the change in atmospheric temperature profile, for the seven channels used in determining the atmospheric temperature profile.

It can be shown that

$$\int W_i(P)\, d\ln(P) \cong 1 - \tau_i(P_s). \tag{5}$$

Therefore, to a good approximation, for two profiles differing by a constant, δ,

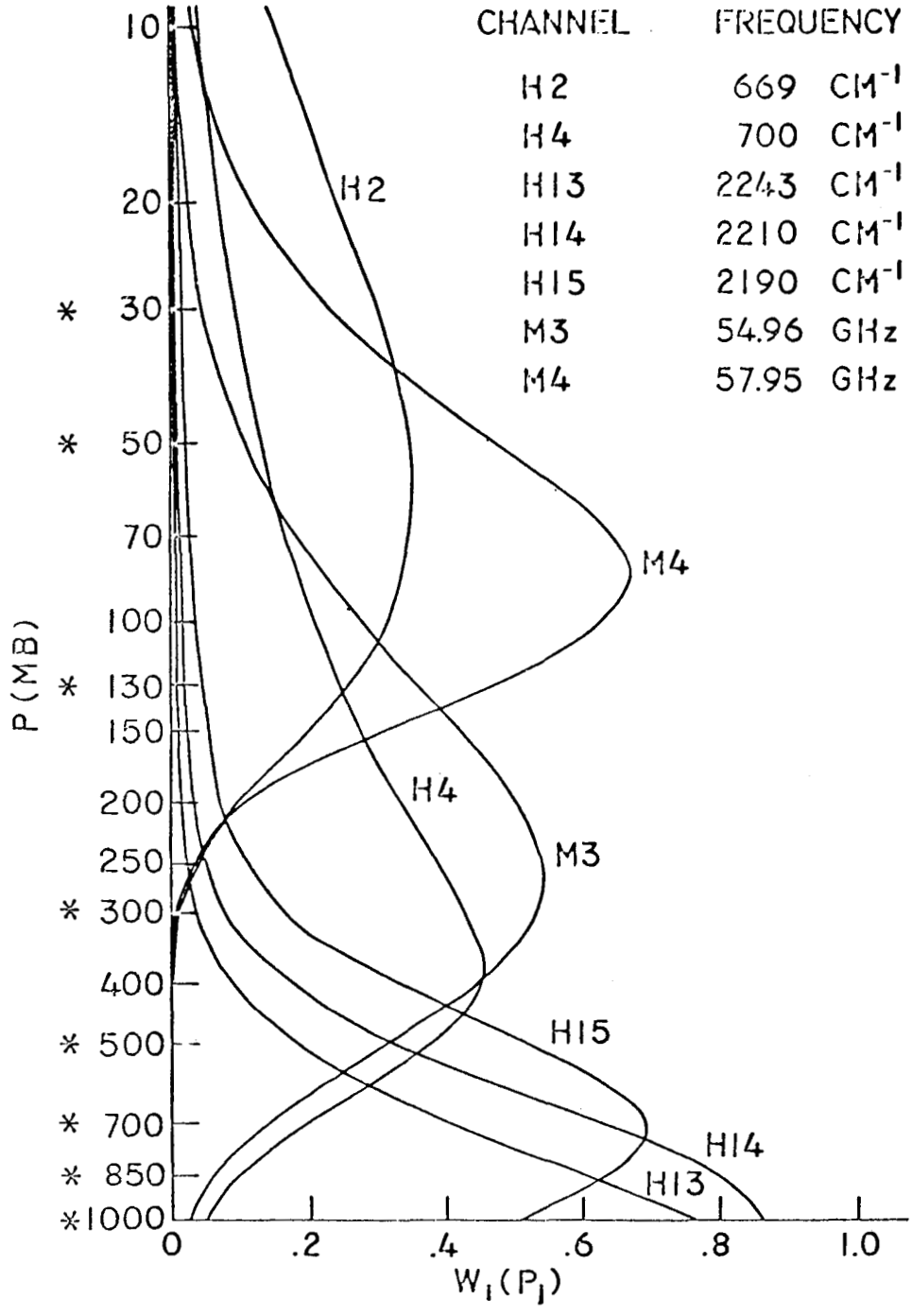

Figure 1. Weighting functions for the seven temperature sounding channels, U.S. standard atmosphere, nadir viewing. Boundaries of the atmospheric layers used in the analysis are marked by*.

$$T_i\,[T(P) + \delta] \cong T_i\,[T(P)] + \delta(1 - \tau_i(P_s)), \tag{6}$$

that is, a constant shift of temperature profile throughout the atmosphere produces approximately the same change in brightness temperature, reduced by a small amount if the channel sees the surface. Moreover, if we look, for example, at channel M4 in Figure 1, we see the brightness temperature in that channel is virtually independent of temperatures above 10 mb and below 300 mb and is mostly dependent on temperatures between 50 mb and 130 mb. Therefore, we can attribute a difference, δ, between observed clear-column brightness temperature, T^N_{M4}, and computed brightness temperature, T^N_{M4}, to a comparable difference in the true mean temperature in the layer between 130 mb and 50 mb, $\bar{T}_i = \int T(P)\, d\ln P$, and that of the Nth guess. In the analysis, differences in mean layer temperatures between the slabs shown with boundaries marked by * in Figure 1 are taken as a weighted sum of differences between observed and computed brightness temperature according to

$$\bar{T}_i^{N+1} = \bar{T}_i^{N} + \Sigma_j \bar{W}_{ij}\,[\hat{T}_j^{N} - T_j^{N}]/\Sigma_j \bar{W}_{ij} \tag{7}$$

where $\bar{W}_{ij}$ is the average value of $W_j(P)$ in layer i. The weighted sum over all channels is taken to reduce noise and stabilize the solution.

Equation 7 defines (N+1), the estimates of mean layer temperatures in seven atmospheric layers between 1000 mb and 30 mb. This is insufficient to uniquely determine a total temperature profile $T^{N+1}(P)$ or even layer mean temperatures between the nine mandatory levels reported operationally by NESS. To insure uniqueness, a constraint is now put on the system that

$$T^{N+1}(P_j) = T_G(P_j) + \sum_{k=1}^{L} A_k^{N+1} F_k(P_j) \tag{8}$$

where $T_G(P)$ is a global mean temperature profile, $F_k(P)$ are empirical orthogonal functions extending from 1000 mb to 30 mb, given by the eigenvectors, with largest eigenvalues of the covariance matrix of 800 global radiosonde profiles, and A_k^{N+1} are iterative coefficients.

The L coefficients, A_k^{N+1}, can be determined for each iteration from the N+1 estimate of mean layer temperatures, $\bar{T}^{N+1}$. If for example, we want to find the L coefficients that compute mean layer temperatures that agree to the M specified values best in a least square sense, then

$$A^{N+1} = (F'F)^{-1} F'\Delta^{N+1} \tag{9}$$

where A is the vector of L coefficients, F is an M by L matrix with elements F_{ik} given by the mean value of $F_k(P)$ in layer i, and Δ_i^{N+1} is the difference between $\bar{T}_i^{N+1}$ and $\bar{T}_{G,i}$, the mean layer temperature of the global mean.

$$\Delta_i^{N+1} = \bar{T}_i^{N+1} - \bar{T}_{G,i}$$

Because of uncertainties in the mean layer temperatures, increased stability is obtained by finding coefficients minimizing a combination of the difference between estimated and computed mean layer temperatures, on the one hand, and the total variance of the solution on the other hand. The appropriate equation is given by

$$A^{N+1} = [F'F + \gamma H]^{-1} F' \Delta^{N+1} \tag{10}$$

where H is a diagonal M x M matrix with H_{ii} being the inverse of the fraction of total variance arising from eigenvector i and γ is a constant. In practice, equation 10 was used with six EOFs and $\gamma = 5 \times 10^{-4}$.

The net result of equations 7, 8, and 10 is an equation of the form

$$T^{N+1}(P_j) = T^N(P_j) + \Sigma_i B_{ji}^N [\hat{T}_i^N - T_i^N]. \tag{11}$$

The form of this equation, relating an increment in temperature at any pressure as a linear combination of observed and computed brightness temperatures for the temperature sounding channels, is identical to that used in a statistical regression analysis. There are several very important differences however. Foremost among these is that B_{ji} is computed with every iteration, based on the profile, and not selected a priori, perhaps as a function of location and time, on the basis of empirical relationships. Moreover, every term in equation 11 is iteration-dependent, including the clear-column brightness temperatures. The matrix B is a function of many factors, including the statistical matrix F, used only as a constraint on the solution. The matrix F of empirical orthogonal functions is taken once and for all. Unlike in the regression method, there is no need for special statistics as a function of geographic location or time of year.

4. Accounting for Effects of Clouds on the Infrared Observations

The infrared radiance observed in an otherwise homogeneous field of view containing partial homogeneous cloud cover α, is given, by a reasonable approximation, as

$$R_i = \alpha R_{i,CLD} + (1 - \alpha) R_{i,CLR} \tag{12}$$

where $R_{i,CLD}$ and $R_{i,CLR}$ are the radiances which would have been observed if the field of view was completely cloudy or clear, respectively. Computation of clear-column radiances $R_{i,CLR}$ can be done routinely as in equation 1, but computation of $R_{i,CLD}$ requires accurate knowledge of the optical as well as the meteorological properties of the cloud. It is more advantageous to be able to account for the effects of clouds indirectly than to have to model their radiative transfer properties. As shown by Chahine (1974), an estimate of the clear-column radiance, R_i, can be reconstructed from the observations in adjacent fields of view according to

$$\hat{R}_i = R_{i1} + \eta[R_{i,1} - R_{i,2}] \tag{13}$$

where $R_{i,j}$ is the observation for channel i in the field of view j and η is given by $\alpha_1/(\alpha_2 - \alpha_1)$, with $\alpha_2 > \alpha_1$. Since η is dependent only on fractional cloud cover, η is independent of channel and spectral region. Once η is determined, clear-column radiances can be reconstructed from the observations by using equation 13. An estimate of η is obtained with each iteration.

It is seen from equation 13 that large values of η will tend to amplify noise in the observations and are, therefore, undesirable. In the other extreme $\eta = 0$ implies field of view 1 is clear and $\eta = -0.5$ is taken when it appears both fields of view are clear. As shown by Chahine (1974) and Halem *et al.*, (1978), η can be determined as part of an iterative scheme according to

$$\eta^N = \frac{R_7{}^N - R_{7,1}}{R_{7,1} - R_{7,2}} \tag{14}$$

where $R_7{}^N$ is the computed clear-column radiance for the 15 μm surface channel, using the Nth iterative temperature profile. The scheme will converge provided only 4.3 μm infrared channels are used for temperature sounding in the lower troposphere. The rate of convergence increases with the difference between the surface temperature and the cloud-top temperature. Under some high noise, low contrast conditions, divergent solutions can occur in the sense that an overestimate of η^N will cause an overestimate of the reconstructed 4.3 μm clear-column radiances which, in turn, will yield an increased lower tropospheric temperature, produce an increased value of $R_7{}^{N+1}$, and lead to an increased η^{N+1}, etc.

When a lower tropospheric-sounding microwave channel is available, such as channel M2, a superior method for determining η can be used, alleviating the need for use of 15 μm channels, which are significantly affected by H_2O and O_3 absorption, in cloud filtering. η is determined as in equation 14 but with the 4.3 μm surface channel, 13, used instead of channel 7. The microwave channel is used to correct errors in $R_{13}{}^N$ due to errors in the iterative temperature profile. The error in η^N from equation 14, is a result of either such an error due to a wrong temperature profile, computational uncertainties such as the effect of water vapor on the transmittance functions of channel 13, observational errors in $R_{13,i}$, or errors in the assumption of only one degree of non-homogeneity in the combined fields of view. The error in $R_{13}{}^N$ due to a wrong temperature profile can be well accounted for by adjusting the computed brightness temperature for channel 13 by the difference in the observed and computed microwave brightness temperatures for channel M2 according to

$$T_{13} - T_{13}{}^N = T_{M2} - T_{M2}{}^N \tag{15}$$

where T_{M2} and $T_{M2}{}^N$ are the observed and calculated microwave brightness temperatures, $T_{13}{}^N$ is the calculated clear-column brightness temperature for channel 13, and T_{13} is the corrected clear-column brightness temperature for channel 13. The corrected clear-column radiance for channel 13 is given by

$$R_{13}{}^{N} = B_{13}\,[T_{13}{}^{N} + (T_{M2} - T_{M2}{}^{N})] \tag{16}$$

and η is now computed according to

$$\eta^{N} = (R_{13}{}^{N} - R_{13,1})/(R_{13,1} - R_{13,2}) \tag{17}$$

If $\eta^{N} \leqslant 0$ and $|T_{13,1} - T_{13,2}| \leqslant 1°K$, η is then taken as -0.5, that is both fields of view are considered clear. This procedure not only speeds up convergence under all conditions, but stabilizes the solution in the sense that an increase in the iterative temperature profile in the lower troposphere will not, to a first approximation, cause an increase in η.

5. Determination of Surface Temperature

Given η^{N}, the clear radiances for the two 3.7-μm window channels, 18 and 19, are reconstructed according to equation 13. Both channels are relative atmospheric windows and are sensitive primarily to the surface (ground) temperature. The two 3.7-μm window channels are superior to the 11-μm window for surface temperature determination because they are more sensitive to surface temperature and less sensitive to uncertainties in surface emissivity and atmospheric water vapor than the 11-μm window channel. They have the disadvantage of being affected by solar radiation during the day, which must be accounted for before accurate surface temperatures can be calculated. At night, surface temperatures are taken to be the average of the surface temperature as determined from channels 18 and 19 where

$$T_{s,i}{}^{N} = B_{i}^{-1}\left[\frac{\hat{R}_{i}{}^{N} - (1 - \epsilon_{i})\,R_{i}{}^{N}{\downarrow}\tau_{i}{}^{N}(P_{s}) - \int B_{i}(T^{N})\,d\tau}{\epsilon_{i}\,\tau_{i}{}^{N}(P_{s})}\right] \tag{18}$$

In general, $T_{s,18}$ and $T_{s,19}$ are found to agree with each other to 1°, even under partially cloudy conditions.

During the day, the effects of solar radiation on the 3.7-μm channels must be accounted for in obtaining accurate surface temperature retrievals from these channels. This can be done directly by subtracting $\rho'_{i}H_{i}\tau_{i,s}(P_{s})$ from $R_{i}^{(N)}$ and substituting the result into equation 18. $H_{i}\tau_{i,s}(P_{s})$, the mean solar radiation across the channel, traversing the path from the sun to the earth and back to the satellite, can be well estimated as $2.16\pi \times 10^{-5}\,B_{i}[5600\ K]\,\cos\theta_{H}\tau_{i}\,(P_{s}, \theta_{H} + \theta)$ where θ_{H} is the solar zenith angle and the transmittance is computed at an effective zenith angle given by the sum of the solar and the satellite zenith angles.

The danger in such a procedure is the uncertainty in ρ'_{i}. If the surface is Lambertian and the emissivity is known, ρ'_{i}, the directional reflectance, is equal to $(1 - \epsilon_{i})/\pi$. Significant errors of up to a factor of 2 can be made in these estimations of ρ'_{i}, which may produce errors of up to 10°K in retrieved surface temperature. These errors arise from uncertainties in ϵ_{i} and the non-Lambertian

character of the surface. The same uncertainties in ϵ_i, however, do not appreciably affect the calculated thermal radiation, and estimated values of 0.85 over land and 0.95 over ocean are used in the analysis. T_s and ρ' are solved for in an iterative manner.

For 3.7 μm sounding channel i, we can write

$$\frac{R_i^N - R_{ATM,i}^N}{\epsilon_i \tau_i^N (P_s)} = B_i(T_s) + d_i H_i\downarrow = A_i^N \tag{19}$$

where $R_{ATM,i}$ is the atmospheric contribution to the calculated clear-column radiance, $d_i = \rho'_i/\epsilon_i$, and $H_i\downarrow$ is the effective solar radiation striking the earth. The left-hand side of equation 19, and consequently A_i, is known in a given iteration. Assuming ρ'_i and ϵ_i are the same for both 3.7-μm channels, one obtains the equation

$$B_i(T_s) - \alpha B_j(T_s) = A_i - \alpha A_j = A \tag{20}$$

where $\alpha = H_i\downarrow/H_j\downarrow$. This non-linear equation in one unknown, T_s, is solved for iteratively according to

$$\frac{e^{-h\bar{\nu}/T_s^{M+1}}}{e^{-h\bar{\nu}/T_s^{M}}} = \frac{A}{B_i(T_s^M) - \alpha B_j(T_s^M)} \tag{21}$$

where $\bar{\nu} = (\nu_i + \nu_j)/2$. This procedure converges rapidly. Once T_s is determined, d is calculated from equation 19 and the appropriate value of ρ' is used in equation 1 to correct the 4.3-μm channels for reflected solar radiation effects. Ground and sea surface temperatures and temperature profiles produced during the day appear to be of comparable quality to those produced at night.

6. Data Processing and Retrieval Scheme

GLAS has processed TIROS data in both a pseudo-operational and high-resolution mode. The pseudo-operational model produces a sounding every 250 x 250 km. HIRS2 observations are grouped in 125 x 125 km areas. Observations in each area are further separated into two 'fields of view' of equal number of spots according to the warmest and coldest values of the 11-μm window channel 8. Observations of spots in each field of view are averaged for each channel. Microwave observation from the closest MSU spot are assigned to the 125 x 125 km area. The sounding in a 250 x 250 km area is done in the 125 x 125 km area with the warmest value for the channel-8 brightness temperature. Initial conditions for that sounding are taken as the 24-hour NMC analysis interpolated in space to the appropriate location. The high-resolution runs are performed on the McIDAS system in an analogous way, except one sounding is performed in a 2 x 2 quadrant of a 4 x 4 array of HIRS spots.

Given initial conditions and satellite observations, a sounding is produced by the following sequence of computations:

1. Compute microwave emissivity ϵ^0, from the initial guess, $T^0(P)$ with the initial-guess ground temperature equal to the initial-guess air temperature.

2. Calculate η^0 using the initial guess profile, the computed microwave emissivity, and the observed radiances in channels 13 and M2.

3. Construct clear-column radiances for the 3.7-μm channels using η^N and determine a ground temperature T_S^N.

4. Recompute microwave emissivity, ϵ^N, using T_S^N and $T^N(P)$.

5. Recalculate η^N.

6. Compute reconstructed clear-column brightness temperature $\hat{T}^N$, clear-column brightness temperatures T^N, and the new temperature profile $T^{N+1}(P)$.

7. Compute the root mean square difference between reconstructed and computed clear-column brightness temperatures for the seven temperature sounding channels, D^N, and compare to D^{N-1}.

8. If $D^N < 0.95\ D^{N-1}$, convergence has not been reached, and return to step 3. Otherwise, if $D^N < 1°K$ and the difference of observed and computed brightness temperatures for microwave channel 2 is less than $1°K$, $T^{N+1}(P)$ is taken as the solution. If the above two conditions are not met, the retrieval is rejected. Convergence is usually achieved in 3 to 6 iterations. Overall, approximately 70 percent of the global retrievals are accepted.

7. Results

Pseudo-operational mode retrievals were run for the period Jan 4 to Feb 25, 1979. The accuracy of the retrievals was verified against measurements from a set of global oceanic radiosondes colocated in space to 150 KM and in time to 3 hours. Accuracies of mean temperatures in the layers reported operationally by NOAA/NESS were computed for both NESS and GLAS soundings and are shown in Table 2. The first two columns refer to RMS errors of soundings in areas which NESS felt were too cloudy for use of the tropospheric sounding HIRS channels and only MSU tropospheric soundings were performed. The second two columns refer to partially cloudy areas in which all MSU and HIRS2 channels were used in the analysis by NESS, but with a cloud correction for HIRS2 radiances. The last two columns refer to soundings in areas NESS treated as clear. GLAS soundings always used the seven HIRS 2 and MSU channels shown in Figure 1. In all cases, the GLAS and NESS soundings were within 200 km of each other. Examination of Table 2 shows the

Table 2
RMS Mean Layer Temperature Retrieval Accuracies (°K);
Jan 4 to Feb 25, 1979; Global Oceanic Radiosondes

Layer MB	NESS Cloudy		NESS Partially Cloudy		NESS Clear	
	GLAS	NESS	GLAS	NESS	GLAS	NESS
70 – 50	1.39	1.18	1.33	1.73	1.84	1.82
100 – 70	1.44	1.59	2.17	2.41	1.71	2.12
200 – 100	1.53	1.72	1.62	1.82	2.26	1.81
300 – 200	2.90	3.20	1.99	2.75	1.55	1.54
400 – 300	2.31	2.34	2.48	2.75	2.00	1.96
500 – 400	2.06	2.35	1.64	2.39	1.67	2.05
700 – 500	1.75	2.46	1.35	1.90	1.55	1.70
850 – 700	2.36	3.04	2.11	2.04	1.69	1.89
1000 – 850	2.95	3.11	2.72	2.61	2.39	2.57
OVERALL	2.20	2.52	2.00	2.32	1.86	1.94

GLAS tropospheric soundings to be of higher accuracy than those of NESS for all cases, especially in partially cloudy and cloudy cases. It is also observed that the general quality of the soundings decreases with increasing cloudiness, but much more so in the case of NESS soundings than in GLAS.

Table 3 summarizes the overall RMS errors of the GLAS and NESS soundings, but this time also breaking down the NESS statistics into errors for soundings in areas where GLAS accepted the retrieval (≈70 percent of the total for each sounding area) and areas for soundings in areas rejected by GLAS. It is apparent from Table 3 that in areas where NESS used the HIRS2 channels and GLAS accepted the retrieval, results of comparable accuracy were obtained. In those areas where the GLAS scheme indicated a problem, the NESS retrievals were of considerably lower quality for both clear and partly cloudy cases. The partly cloudy retrievals in areas rejected by GLAS are of particularly low quality, perhaps due to problems of multiple cloud functions in these areas. In the areas in which NESS utilized only MSU channels for tropospheric soundings, considerable degradation of results is found relative to GLAS in both categories. This is due primarily to the comparatively low information content in the MSU tropospheric sounding channels relative to those of HIRS2, even under extensive, but not total, cloud cover.

Studies with high-resolution soundings on the McIDAS have just begun. Two cases have been done, Jan 11 0Z, off the west coast of the United States, and Jan 11 4Z, off the west coast of Europe. In the first case, it was found, surprisingly, that very significant differences occurred in the

Table 3
Overall Mean Layer Temperature RMS Errors;
Global Oceanic Statistics Jan 4 to Feb 25, 1979

NESS Retrieval Type	GLAS	NESS GLAS Accepts	NESS GLAS Rejects	NESS All
Clear	1.86	1.80	2.27	1.94
Partially Cloudy	2.00	1.97	2.82	2.32
Cloudy	2.20	2.48	2.61	2.52
All	1.96	1.98	2.51	2.16

pattern of the 300 to 1000-mb thickness contours obtained by the GLAS method of analysis, and those obtained by the method used to produce the "enhanced" soundings as part of the Special Effort. Unfortunately, there was insufficient radiosonde information to validate either of the patterns. The second case, shown in Figure 2, contains many radiosonde reports, indicated as large numbers in the figure, showing measured 1000 to 300-mb thickness in decameters. The dashed contour field corresponds to that of the GLAS retrievals and the solid field corresponds to that of the enhanced soundings. In this case, the patterns are in fact quite similar qualitatively, but significant quantitative differences occur. Comparison with radiosonde verification indicates better general agreement in the case of the GLAS soundings. The sources of the differences, particularly in the case of large qualitative pattern differences, are being investigated.

References

1. Chahine, M. T., J. Atmos. Sci., 27, 960-967 (1970).

2. Chahine, M. T., J. Atmos. Sci. 31, 233-243 (1974).

3. Halem, M., Ghil, M., Atlas, R., Susskind, J., and Quirk, W. J., NASA Tech. Memo. 78063, 2-28 to 2-33 (1978).

4. Kornfield, J., and Susskind, J., Mon. Wea. Rev. 105, 1605-1608 (1977).

5. Mo, T., and Susskind, J., NASA Tech. Memo. 80253, 81-87 (1978).

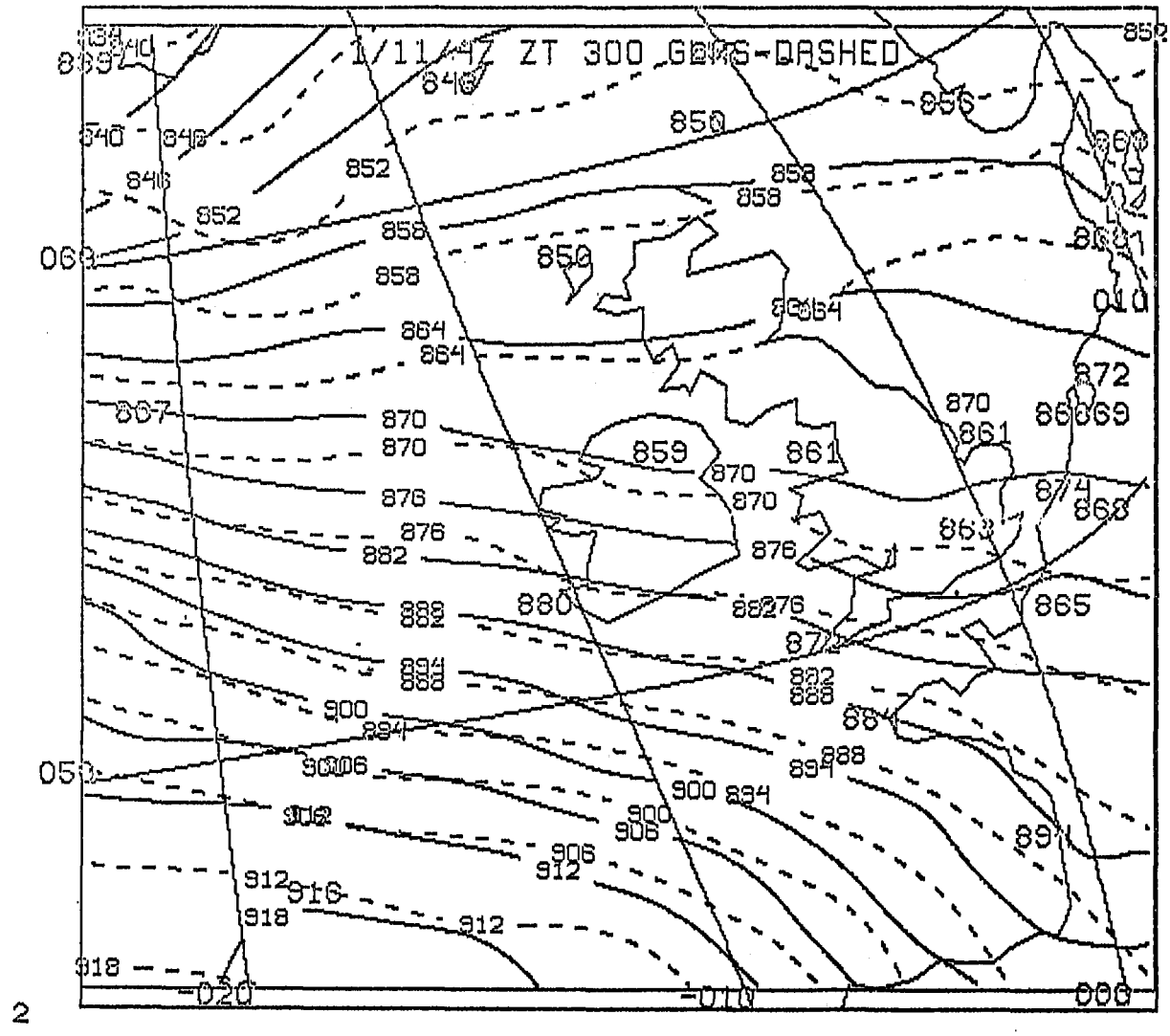

Figure 2. 300 to 1000-mb thickness fields off the coast of Europe, Jan 11, 4Z. Large numbers indicate radiosonde reports, Jan 11 0Z, of thicknesses in decameters. Dashed contours are for GLAS retrievals. Solid contours are for enhanced retrievals.

6. Rosenkranz, P. W., IEEE Transactions on Antennas and Propagation, 23, 498-506 (1975).

7. Susskind, J., Halem, M., Edelmann, D., Tobenfeld, E., Searl, J., Karn, R., Dilling, R., Sakal, D., Tung, L., Carus, H., Rushfield, N., and Tsang, L., NASA Report X-1130-77-53, Appendix A (1977).

LOW-LEVEL MOISTURE FROM VAS

Christopher M. Hayden
NOAA/NESS
Madison, Wisconsin

1. Introduction

The history of atmospheric moisture sounding from satellites is not encouraging. Good success has been achieved only in terms of total precipitable water (Staelin *et al.*, 1976, Shen and Smith, 1973). Some skill has been shown for defining moisture in deep layers (Smith and Howell, 1971), but detailed vertical moisture profiling has not been possible with either real or theoretically simulated data.

Our inability to sound the atmospheric moisture has not been a serious detriment to the application of satellite data in synoptic meteorology. However, as we now direct attention to the VISSR Atmospheric Sounder (VAS), whose mission is the early detection and definition of potential severe weather on the subsynoptic scale, the moisture problem becomes more important if not dominant. With the launch of the first VAS imminent, it is highly relevant to readdress the question of our capacity to sense moisture from space measurements.

The TIROS-N sounder is a close analogue to what will fly on GOES-D and can be used to investigate the probable capability of VAS. Basically, there are three frequencies applied to sensing moisture in the troposphere. This paper will assess the ability of these three measurements to define the moisture pattern. It can be stressed at the outset that results show the outlook is not as gloomy as might be expected from past studies. It is certainly true that one cannot achieve the detail available with a radiosonde hygristor. Sharp discontinuities cannot be sensed by a passive sounder, especially since the measurement tends to "saturate" with the first moisture layer encountered. However, the satellite measurements demonstrate a high degree of skill in defining the horizontal gradient. Moisture "tongues" and "dry lines" are readily delineated with some, perhaps two layers, of vertical definition. These attributes allow both the calculation of important advective quantities as well as (in concert with the temperature sounding) a gross definition of the vertical stability. The skill is demonstrably commensurate with subsynoptic forecast models and perhaps even to regional-scale models.

2. Retrieval Method

The retrieval technique that is currently being used for man/computer interactive soundings by the NESS group in Madison, Wisconsin is basically statistical, but involves correctly identifying and removing the surface contribution to the measurements. Temperature and moisture profiles are

obtained solely from the atmospheric component using simple multiple regression. The regression coefficients are obtained from a dependent sample of current radiosonde measurements regressed against brightness temperatures calculated from the same radiosonde measurements with an added realistic instrumental noise estimate. The motivation for treating the atmosphere instead of the total radiance is to sensitize the statistics at low levels, especially for moisture determination.

The signal received at frequency ν by the satellite under clear sky conditions can be expressed by

$$I_c(\nu) = I_s(\nu) - \int_0^{p_s} B(\nu, t) \frac{d\tau}{dp} dp \qquad (1)$$

where $I_s(\nu)$ is the surface contribution, p_s is the surface pressure, $B(\nu, t)$ is the Planck radiance, and $d\tau/dp$ is the "Planck radiance profile" weighting function. Variations in surface emissivity, reflectivity, and elevation cause considerable uncertainty in the interpretation of measurements which have a surface contribution. Also, the surface term is a function of the surface skin temperature, which may be considerably different from the usual meteorological parameter, the shelter air temperature. Failure to recognize and appropriately account for the surface contribution can lead to temperature profile errors throughout the troposphere. For moisture sounding, the proper definition of the surface term is even more important. Not only do the same terrain induced uncertainties exist as in the case of temperature sounding, but changes in the surface and atmospheric contributions tend to compensate as the low-level moisture varies. In general, as the low-level moisture increases, the atmospheric component increases. However, the total transmittance decreases, so the surface contribution decreases.

The consequence of using the atmospheric component as opposed to the total signal is that the variance which depends on atmospheric properties is greatly enhanced, especially with respect to moisture. For example, Table 1 gives the simulated signal for those TOVS channels that sense the surface with and without surface contribution for a normal and dry (10 percent relative humidity) radiosonde profile shown in Figure 1. Note in particular that the atmospheric component of the most transparent water vapor channel (8.3 μ) changes by almost 20 degrees when the water content is reduced, whereas the total signal changes by only 2.3 degrees. Similarly, for the 13.4-μ channel (which is quite sensitive to moisture although it is generally thought of as a temperature sounding channel) the moisture induced changes are 11.3 versus 1.4 degrees.

The increased variance is readily shown to produce increased skill in retrieving water vapor profiles, at least in simulation tests. Table 2 presents a comparison of using full versus atmospheric components on an independent sample of simulated (from radiosonde profiles) brightness temperatures taken during July 1980. (Coefficients were generated from a separate radiosonde sample taken during the same period.) The table gives both RMS statistics and explained variance for layers which are used in the moisture deviation. Predictors used in the regression are measurements at 14.0, 13.7, 13.4, 8.3, 7.3, 6.7, 4.57, 4.52, 4.46, 4.40 μm as well as estimates of the surface pressure, temperature, and dewpoint, which are routinely obtained from surface stations and used in the retrieval process. The surface data for the statistics presented in Table 2 are obtained directly from

Table 1
Comparison of Simulated Brightness Temperature for Radiosonde of Figure 2
With and Without Surface Contribution

Channel Frequency	Observed H_2O		10 Percent Relative Humidity	
(μm)	Total	Atmos	Total	Atmos
14.0	247.7	244.5	248.0	243.0
13.7	262.0	252.3	262.7	248.2
13.4	276.0	255.0	277.4	243.7
4.57	284.5	262.4	285.5	259.5
4.52	272.3	259.8	272.7	258.4
8.3	295.4	256.0	297.7	236.4
7.3	267.6	267.1	272.8	268.5
6.7	247.4	247.4	252.6	252.5

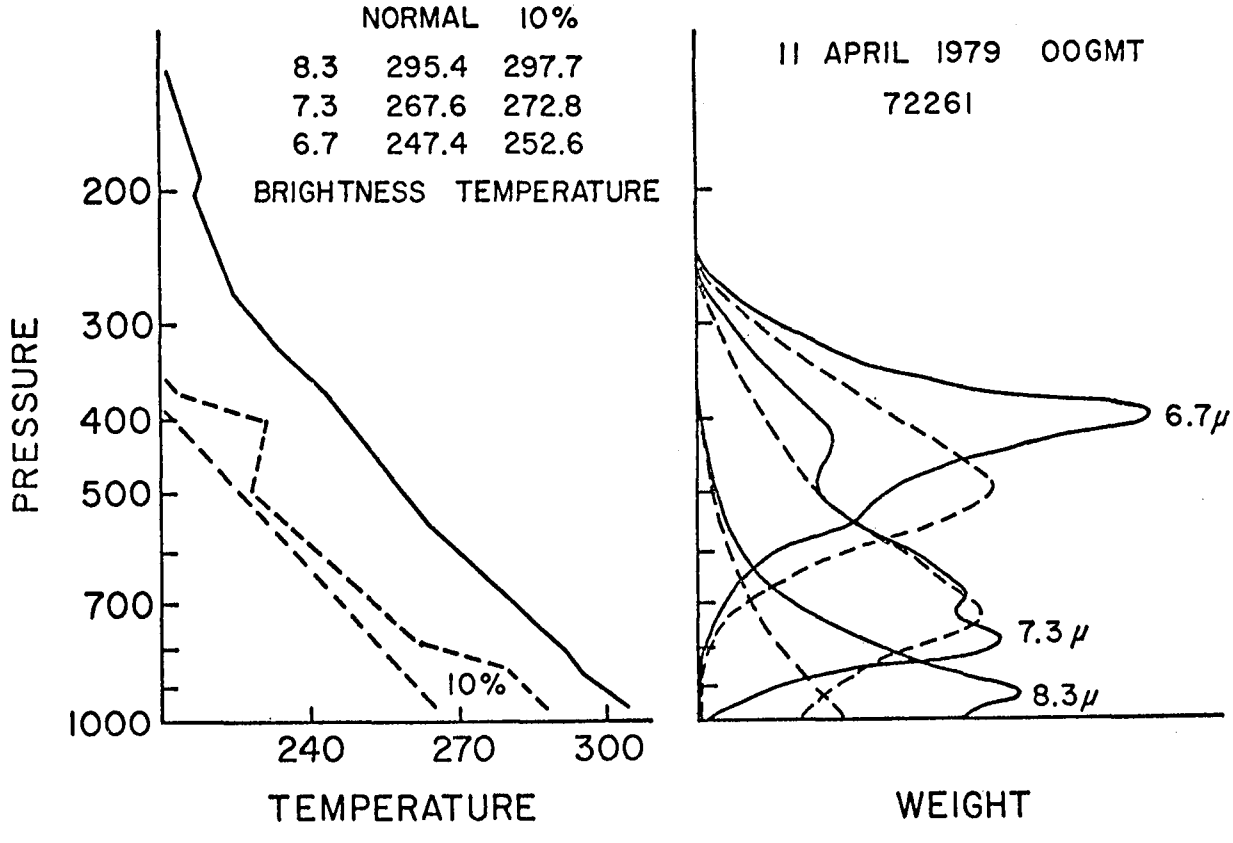

Figure 1. (left) Midlatitude standard atmosphere temperature and dewpoint profile (10 percent humidity profile also shown). (right) Brightness temperature weighting functions for TOVS 6.7 μm water vapor band for profiles shown at left.

Table 2
Independent Sample Comparisons of Moisture Retrievals Obtained With Simulated Brightness Temperatures. Retrievals Use (a) Full Simulated Measurement and (b) Atmospheric Component Only. Statistics are Root-Mean-Square Error and Explained Variances.

Layer	(a)		(b)	
	RMS	EV	RMS	EV
Surface	0.9	0.98	1.0	0.98
Surface – 700	3.2	0.64	2.2	0.84
850 – 500	2.5	0.84	2.5	0.84
500 – 300	1.5	0.96	1.6	0.96
400 – 300	2.7	0.90	2.6	0.91

the radiosonde with noise added. The table depicts a dramatic improvement in the skill at low levels when the atmospheric component is isolated. The explained variance for the surface-to-700-mb level (as estimated by the correlation coefficient) increased from 64 to 84 percent. Other layers not including the surface are only very slightly affected.

One might legitimately question the impact of using the observed surface data to achieve a surprisingly good result in the surface layer. In answer to this, experiments were tried where the surface dewpoint was excluded from the predictors. The results for the full measurement case differed from those of Table 2 at the surface and the lower two layers where the explained variance fell from 98 to 31 percent, from 64 to 43 percent, and from 84 to 78 percent, respectively. The changes for the surface and lower two layers for the atmospheric component case were 98 to 78 percent, 84 to 76 percent and 84 to 74 percent. The conclusion to be drawn is that the observed surface dewpoint for the atmospheric component retrieval is useful but not critical for the prediction or measurement of the low-level moisture. The satellite measurements suffice by themselves to determine the low-level atmospheric layer moisture to a fair degree of accuracy.

The mechanics of removing the surface contribution to the measurements involve estimates of the surface transmittance, the reflected solar contribution (at 4 μm), and the skin temperature. The last is directly measured by a channel at 11.1 μm, assuming that cloud contamination can be recognized and removed. The others are somewhat more difficult to contend with, and must be treated theoretically. Details of this treatment can be found in Hayden *et al.*, (1980). Assuming that methods for obtaining transmittances and cloud cover exist, the general retrieval problem is shown in Figure 2, and the corrected measured (m) atmospheric radiance to which the retrieval statistics are applied is given by

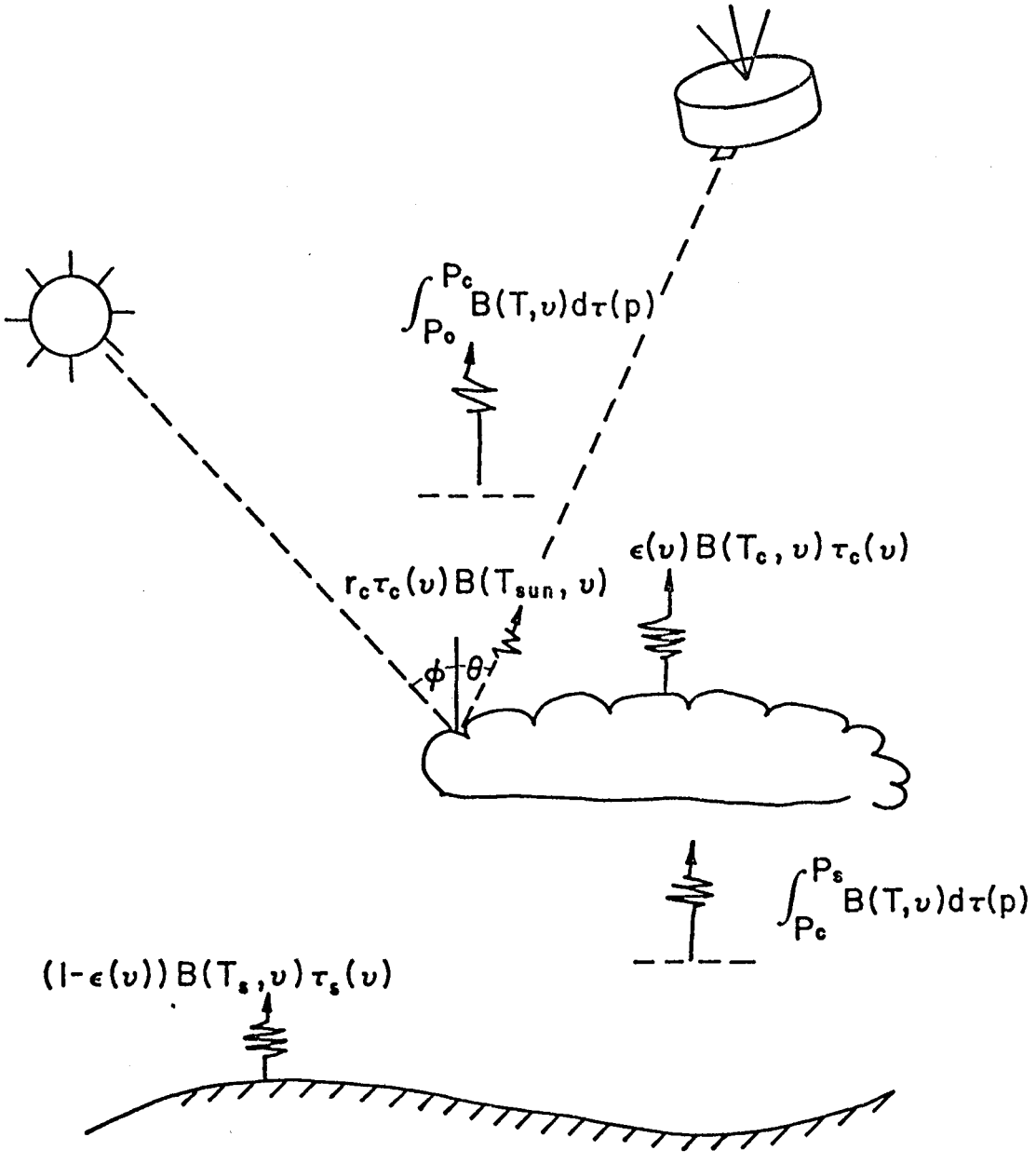

Figure 2. Schematic of components involved in separating atmospheric components from total radiance and for correcting for cloud cover.

$$I_m'(\nu) = I_m(\nu) - \epsilon(\nu)B(\nu, T_c)\,\tau(\nu, p_c) - (1 - \epsilon(\nu))B(\nu, T_s)\,\tau(\nu, p_s) - \epsilon(\nu) \int_{p_c}^{p_s} B(\nu, T)\, d\tau(\nu, p) - SC(\nu), \tag{2}$$

where ϵ is an effective emissivity (for short or long wavelengths) including both true emissivity and cloud amount, B is the brightness temperature, T_c is cloud top temperature, τ is the transmittance, T_s is the surface temperature, and SC is the solar correction which is shown in the figure to include reflectivity of the sun's irradiance.

If the cloud does not exist in the field of view or if it can be eliminated by the adjacent field-of-view technique (Smith, 1969), $\epsilon(\nu) = 0$ and (2) is considerably simplified. In practice, the full equation is required only in areas of substantial cloud cover, which experience (in spring and summer only) shows to yield approximately 10 percent of the total number of retrievals. It should be noted that the 10-percent figure is somewhat misleading in terms of total cloud cover, since retrievals are not made in the presence of extensive high cloud because of the uncertainty involved in estimating the integral term of (2), especially with respect to moisture sounding.

3. Moisture Below Clouds

Since cloud screens infrared radiation, there is essentially no measurement of the moisture existing below the cloud. (Temperature can still be estimated using the microwave measurements and it is in this way that the integral term of (2) is estimated in solving for temperature below clouds.) However, the knowledge that the cloud exists is useful information on the moisture, and this has been put to use by the NESS group at Madison in modeling the moisture below the cloud level.

The cloud model is based on the assumption that the profile of mixing ratio is given by

$$w(p) = w(p_o)\,(p/p_o)^{\lambda}. \tag{3}$$

Surface pressure and mixing ratio are assumed known from conventional surface data. The exponent λ is determined on an individual case basis, assuming that the cloud pressure is known. The field of view of the satellite is not, however, assumed to be overcast. An effective cloud amount is calculated from the 11.1-μm window channel according to

$$N = \frac{B(11.1, T_s) - I_m(11.1)}{B(11.1, T_s) - B(11.1, T_c)}. \tag{4}$$

The mixing ratio at the cloud level is approximated by

$$W_c = NW_s + (1 - N)\hat{W}_c, \tag{5}$$

where W_s is the saturation mixing ratio at the cloud temperature and $\hat{W}_c$ is the first-guess mixing ratio at the cloud pressure derived from (3) with $\lambda = 3$ (a climatalogically reasonable value). Given W_c it is possible to solve (3) with λ as an unknown such that

$$\lambda = \frac{\ell n(\hat{W}_c/W_o)}{\ell n(p_c/p_o)} . \tag{6}$$

The λ derived from (6) is used with (3) to give a new estimate of the moisture profile. Note that unless $\hat{W}_c$ is saturated, (6) will always give an increased moisture at the cloud level. This leads to a smaller value of λ, which generates increased moisture at all lower levels.

4. Case Study

The TIROS-N orbit of approximately 2040 GMT 10 April 1979 over the midwestern United States nearly coincided with the tornado outbreak that caused loss of life and severe property damage at Wichita Falls, Texas. Because this event occurred on a Severe Storm and Mesoscale Experiment (SESAME) day when numerous data in addition to the normal radiosonde and surface coverage were gathered, the TIROS orbit has been the subject of an intense research effort. The main goal of the research has been to improve the temperature and moisture sounding procedures for subsynoptic application in the environment of severe weather. Some results obtained for this case with the system described above are presented here, although again more details are available in Hayden *et al.*, (1980).

Figure 3 presents contour analyses of the 850-mb dewpoint (sfc-700 mb average) for the 10 April orbit from four sources. Figure 3a was derived from retrievals produced shortly after the event. At the time, temperature and moisture retrievals were calculated with the surface term included and there was no special modeling for moisture. In addition, retrieval coefficients were obtained from samples of colocated radiosonde and satellite measurements rather than from radiosonde and simulated satellite measurements. Figure 3b was obtained from retrievals produced using the procedures discussed in this paper with the modeled moisture below cloud. Figure 3c is the moisture field carried by the National Weather Service Limited Fine Mesh (LFM) model 6-hour forecast valid at 18 GMT 11 April. The LFM forecast is purportedly the level dewpoint, but since the model carries only three layers of moisture the field is implicitly a vertical average. Also included on this panel are dewpoints averaged from the surface to 850 mb from the normal radiosondes at 00 GMT 11 April and the special SESAME radiosondes at 2100 GMT (in brackets). Finally, Figure 3d was derived from a retrieval system that roughly approximates the NESS operational system.

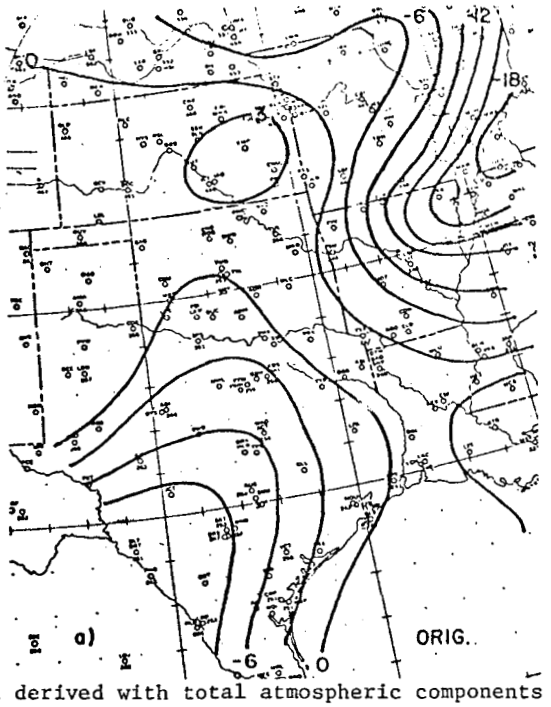

field derived with total atmospheric components and system as of 10 April 1979 from TIROS orbit at 2040 GMT.

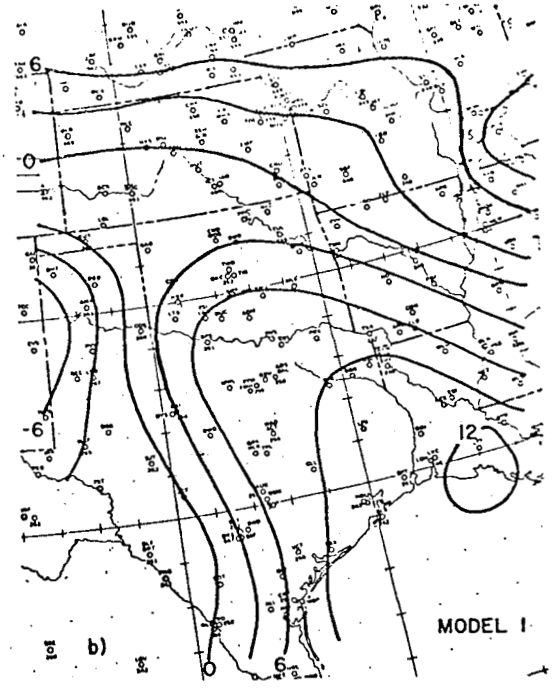

field derived with retrieval system described in text, including moisture model 1.

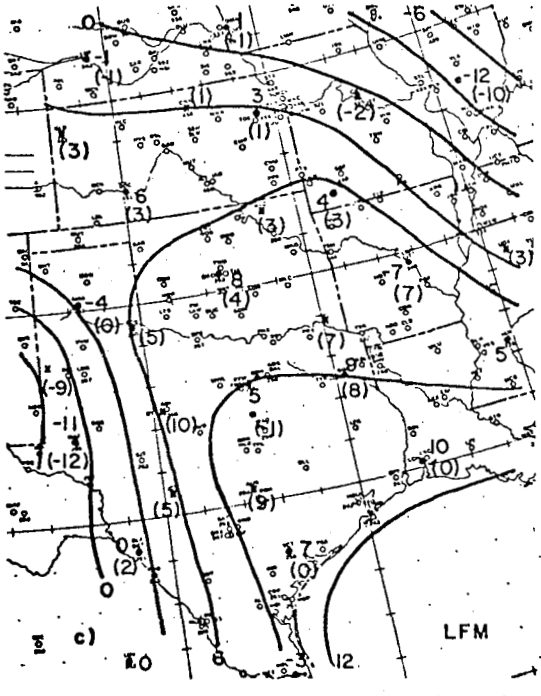

field from LFM 18 GMT forecast with radiosonde reports superimposed. Values in parentheses are special SESAME observations at 2100 GMT, others are from conventional network at 00Z 11 April.

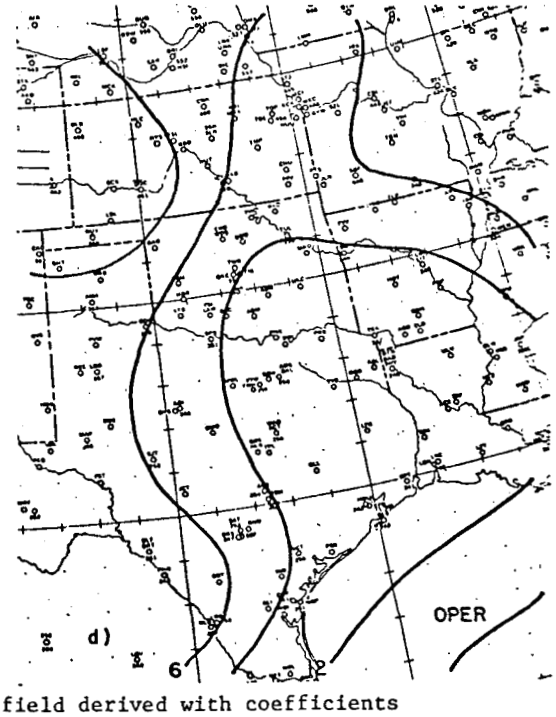

field derived with coefficients approximating NESS operational systems.

Figure 3. Surface to 700 mb average dewpoints for 10 April 1979.

The quality of moisture field obtained with the methods described here is obvious by inspection. It closely resembles the LFM portrayal, although better detail is obtained in the gradients. It is clearly an improvement over the older method (which overemphasized the variance) or the operational method (which is far too smooth). Point comparison with the radiosonde values is futile. There is rough agreement, but the radiosonde values are noisy, at this scale, because of the detailed nature of the measurement.

5. Conclusions

In the current method of moisture sounding used by the NESS group at Wisconsin, no attempt is being made to produce a detailed vertical profile of the atmospheric moisture. Physical limitations of the measurements dictate that only rather broad layers can be sampled. Consequently, this study has presented a mechanism for depicting low and middle tropospheric moisture. In simulation the method is highly successful. In application in a case study the method is certainly credible in describing the moisture in the surface-to-700-mb layer. In particular, the horizontal gradient pattern is well defined and reasonable. Point comparisons with radiosondes show rather large discrepancies, but these can be explained by the different methods of sampling.

This study seeks to show that previous research and current opinion are too pessimistic concerning the capability of defining moisture fields from satellite measurements. Definition may not be adequate for detailed mesoscale modeling, but should be useful to limited area, regional scale models. Looking forward to the advent of sounding from geostationary satellites, hourly updating of the moisture field by a method similar to this should be useful to the subjective short-term forecast as well.

References

1. Hayden, C. M., W. L. Smith and H. M. Woolf, 1980: Determination of Moisture from Polar Orbiting Satellite Sounding Radiances. Manuscript submitted to *J. Appl. Meteor.*

2. Shen, W. C. and W. L. Smith, 1973: Statistical Estimation of Precipitable Water with SIRS-B Water Vapor Radiation Measurements. *Mon. Wea. Rev.*, 101, 24-32.

3. Smith, W. L., 1969: The Improvements of Clear Column Radiance Determination with a Supplementary 3.8 μ window channel. ESSA Technical Memorandum NESCTM 16, U.S. Dept. of Commerce, Washington, DC, 17 pp.

4. ——, and H. B. Howell, 1971: Vertical Distributions of Atmospheric Water Vapor from Satellite Infrared Spectrometer Measurements. *J. Appl. Meteor.*, 10, 1026-1034.

5. Staelin, D. H., K. F. Kunzi, R. L. Pettyjohn, R. K. L. Poon, R. W. Wilcox and J. W. Waters, 1976: Remote Sensing of Atmosphere Water Vapor and Liquid Water with Nimbus 5 Microwave Spectrometer. *J. Appl. Meteor.*, 15, 1204-1214.

STATISTICALLY CONDITIONED LEAST-SQUARES RETRIEVALS PLANNED FOR THE VAS DEMONSTRATION EXPERIMENT

Dennis Chesters
Laboratory for Atmospheric Sciences
NASA/Goddard Space Flight Center

ABSTRACT

Problems in the retrieval of atmospheric profiles from passively observed satellite radiances are reviewed in this paper. Plans are described for statistically conditioned least-squares retrievals of temperature and moisture profiles around mesoscale events, based upon the expected sensitivity of the VAS channels to the atmospheric variations. Simulated soundings for a global data set and for the 1976 National Severe Storm Laboratory (NSSL) severe storm data set are described. This combination of radiance modeling and statistical conditioning should yield reliable mesoscale soundings and provide a test bed for sounding research and development with the VAS instrument.

1. Review of the Passive Retrieval Problem

Information retrieval about the physical conditions along a ray path from the passively observed radiance is well known[1] to be a poorly conditioned[2] problem.[3] It is still an open question whether such retrievals can supply the completeness, resolution, and accuracy needed for detailed numerical models of the atmosphere. Indeed, the fact that any one channel is affected by many independent atmospheric effects is the main justification for flying multi-channel sounding instruments, with each channel having a different relative sensitivity to each effect.

1.1 Overview of Radiation Transfer and Retrievals

Figure 1 views passive sounding as a multivariate remapping problem: there are many independent atmospheric variations and many possible dependent spectral measurements, but we want to infer the atmospheric state from only a few spectral measurements. So, we model the radiation transfer in a few bandpasses with a few atmospheric parameters. Naturally, the filter choice and mathematical parameterization are points of contention, because they can ignore or oversimplify major effects. In any case, passive radiance variations are a relatively insensitive indicator of the detailed atmospheric variations. Many different situations look almost alike and can even be indistinguishable within the observational errors. The main tactics for resolving these ambiguities are to use:

- A good initial estimate for the situation on hand.
- Objective statistical experience to select the most probable conditions consistent with the measurements.
- Quality control in the forms:
  - Consistency checks between the observed and resynthesized radiances
  - Objective propriety checks on the atmospheric parameters (e.g., humidity limits, gradient limits, etc.)
  - Human review of consistency with other data (e.g., visible cloud images, field analyses, etc.).

---

[1] *Remote Sounding from Artificial Satellites,* Houghton , J.T. and Taylor, F. W., Rep. Prog. Phys., 1973, vol 36, 827-919.

[2] *Remote Sensing of the Troposphere,* editor Derr, V. E., Course at the University of Colorado, Boulder, June 1972, printed by NOAA, available from USGPO, Washington, DC 20402.

[3] *Inversion Methods in Atmospheric Remote Sounding,* editor Deepak, A., workshop at Langley Research Center, Hampton, VA, December 1976, available as NASA CP-004, from National Technical Information Office, Springfield, VA 22161.

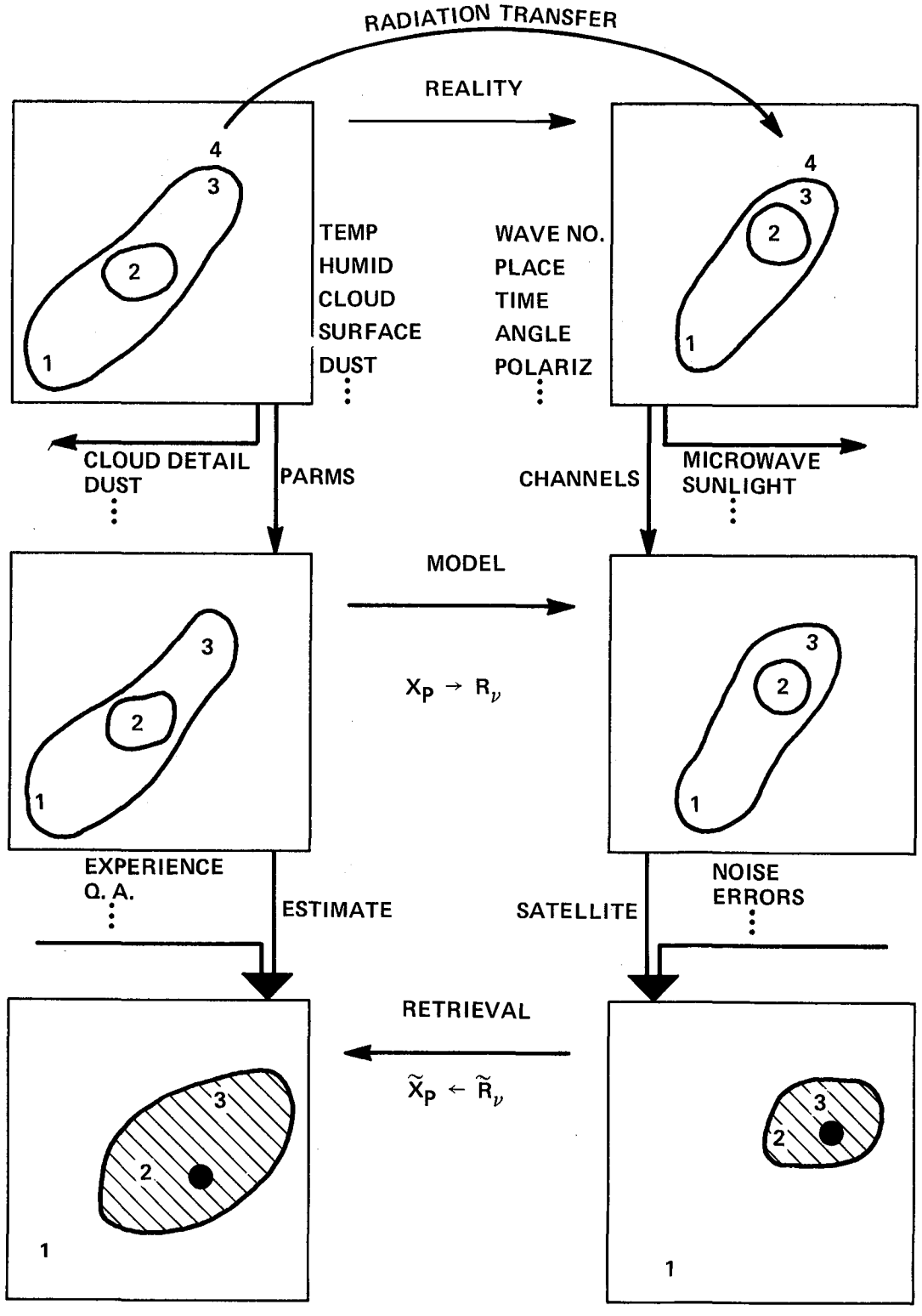

Figure 1. Review of the passive remote sensing problem.

1.2 Problems with Retrievals

Meteorological retrievals using satellite radiances suffer from:

- Poor horizontal resolution with respect to the high-contrast details (mainly clouds)
- A lack of signal (thermal emission) from the tropopause
- The similar appearance of quite variable phenomena (low clouds, humidity, surface height and emissivity, reflected sunlight) at the earth's surface
- Variable aspect (angle from satellite to ground) of the same spot at different times
- Mislocation (navigation and registration errors) in terrestrial coordinates
- Radiance errors (engineering or calibration problems) much larger than the expected random noise
- Radiance insensitivity or ambiguity with respect to the important atmospheric constituents (filter choice)
- Inadequate radiation transfer and retrieval formulation (absorption coefficients or parameterized models) for actual atmospheric conditions.

The VAS instrument on the GOES satellites is expected to do relatively well at timely, well-located mesoscale retrievals compared to the polar-orbiting sounders. At geosynchronous station, VAS is expected to suffer mainly from relatively poor resolution and radiance quality problems.

1.3 Aids to Retrievals

The meteorological retrieval process is supplemented by two classes of atmospheric information to help resolve some of the ambiguities:

- Ancillary data – recent radiosonde and surface reports at nearby sites. These are used as reference values so that radiance variations about the site can be interpreted as corresponding meteorological variations.
- Statistical data – historical observations of atmospheric conditions similar to those being looked at by the satellite. These are used as an ensemble to condition the retrievals to produce the most probable estimate from the set of all other conditions with a similar appearance in the radiances.

This review will concentrate upon the use of statistical data in conditioning a least-squares retrieval scheme based upon physical radiation transfer theory. We hope that the retrievals can benefit both from the reliability of statistical inference and from the analytic flexibility of an optimized physical formulation.

2. Optimized Retrievals from Conditioned Sensitivity Models

The VAS Processor at NASA/GSFC must use a dozen channels of thermal infrared radiances taken from geosynchronous station (GOES-D, -E, -F in 1980, -1, -2), in order to estimate the development of the three-dimensional atmospheric structure during a mesoscale event with space-time resolution of 60 kilometers and 1 hour over a field several hundred kilometers wide. Under good viewing conditions, the retrievals are expected to have a vertical resolution of a few kilometers with an accuracy of ±2°K in temperature and ±25 percent in moisture, based on soundings made with the polar-orbiting instruments.

We expect that the meteorologists using the VAS observations will try to extend the retrieval capability down to a single noisy field-of-view (about 15-kilometer resolution) in difficult areas of cloud cover, surface irregularities and unusual atmospheric conditions. This will require careful interactive processing, with situation-dependent conditioning and quality control by the user himself in the research mode.

We believe that a statistically conditioned least-squares sensitivity inversion scheme is the best objective algorithm for single field-of-view retrievals in recognizable mesoscale weather patterns. The basic constituents of statistically conditioned least-squares retrievals are sensitivity functions and statistical data.

2.1 Sensitivity Functions

A sensitivity function is a functional partial derivative – the response of a channel to a unit change in an atmospheric parameter (e.g., temperature and moisture). The ordinary weighting functions (d_τ(chan)/dlnP) only indicate the sensitivity of a channel's radiance to a unit change in the atmospheric brightness with all other effects held constant. Sensitivity functions have the advantage of being cast in the meteorologist's parameters, of making direct channel-to-channel comparisons easy, and of describing the effect of all significant variables in each atmospheric layer (temperature and moisture content, rather than just local brightness). By converting radiances to brightness temperature and measuring the atmospheric parameters in temperature units, one gets sensitivity functions in the convenient form of degrees Kelvin per degree Centigrade per scale height in the atmosphere: dT*(chan)/dX(P)/dlnP, where X(P) is layer temperature, moisture, etc.

Figure 2 compares the ordinary weighting functions to the sensitivity function of a 13-micron channel on VAS, where one can see that:

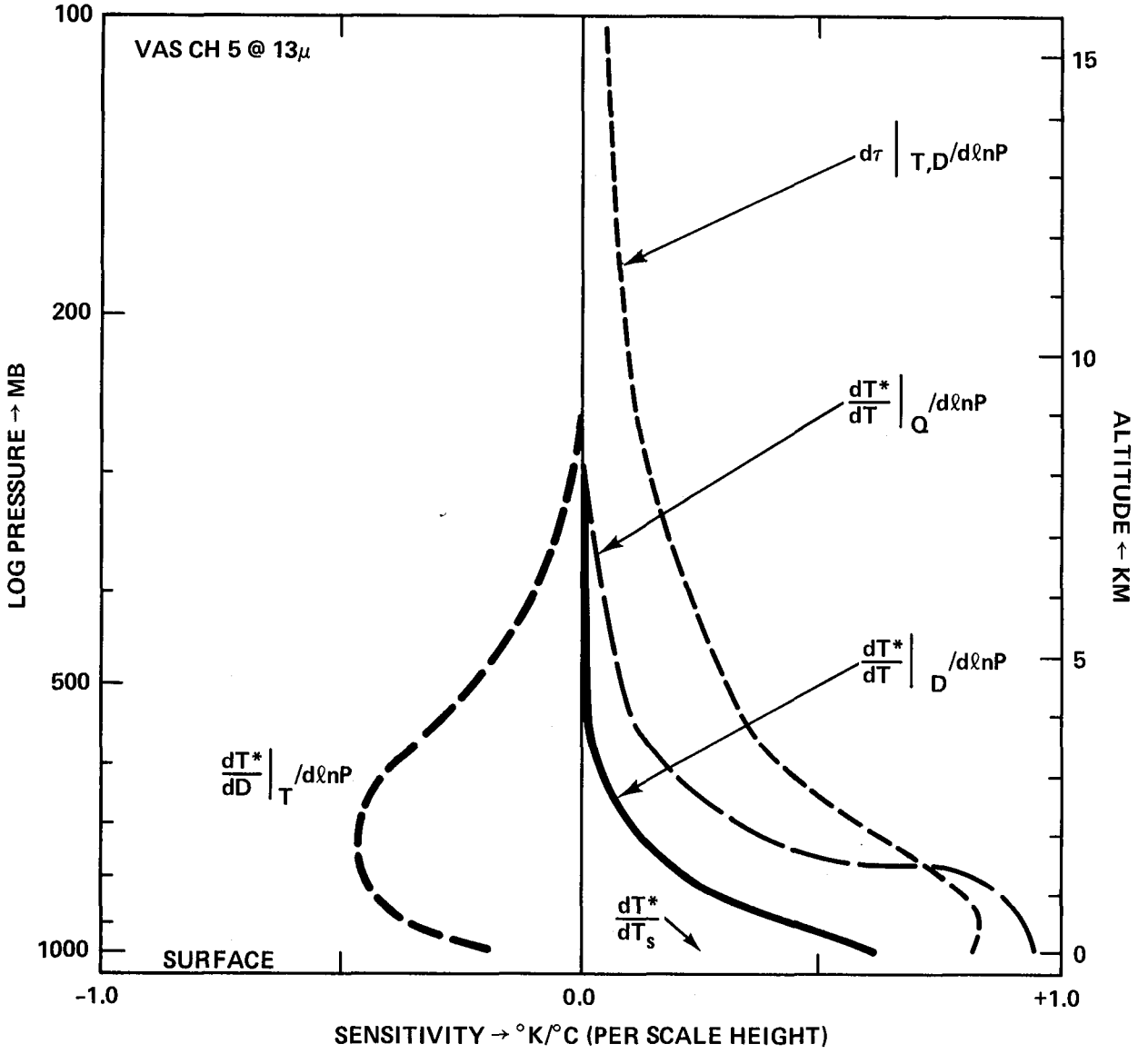

Figure 2. Sensitivity and ordinary weighting functions.

- Greater brightness of the lower atmosphere enhances the sensitivity there
- Channel has roughly equal and opposite sensitivity to independent temperature or dew-point increases at 700 mb due to the radiance absorption by more water at fixed temperature
- Temperature sensitivity looks different if one fixes mixing-ratio instead of dewpoint-depression as the independent moisture parameter in a layer

- Sensitivity to surface brightness temperature variations is included as well.

Temperature-sensitivity functions include the effect upon the local absorption coefficients in addition to the local brightness field. Consequently, the sensitivity of some channels can show the paradoxical effect of having an increase in temperature at the tropopause actually produce a net decrease in the channel's brightness due to the increase in the absorption of the upwelling radiance at this very cold, dim layer.

Sensitivity functions are necessary to minimize the errors in a linearized multi-parameter retrieval algorithm. They convey information about each channel's view of all processes competing for radiation within the same layer, so that one can solve simultaneously for all parameters. It is still a matter for research to extend the method to large nonlinear effects (mainly clouds) or to show that iteration with linearized cloud parameters will converge correctly. Similarly, the sensitivity functions (especially the moisture sensitivity) are somewhat situation dependent, so that one must have either an array of sensitivity functions for different reference conditions (e.g., tropical oceans and mid-western storms) or have a scheme for updating them to the current ancillary data conditions.

2.2 Meteorological Statistical Data

If one has historical data (e.g., radiosondes) at several sites at several times for several events of the same kind (e.g., midwestern thunderstorms), then one can collate one's experience into useful objective numerical forms: mean value profiles and covariance matrices. The mean value profiles serve as reference values for estimating sensitivity functions. The covariances are used to condition the inverse of the sensitivity functions to resolve retrieval ambiguities in favor of the most probable values that can be determined within the radiance errors of the sounding instrument.

It is the meteorologist's own responsibility to acquire the historical atmospheric observations and to use them appropriately.

The vertical correlations are an important factor in improving the vertical resolution and accuracy of remote soundings. It should be possible to show that the horizontal correlations will also improve the corresponding resolution and accuracy of entire fields of soundings, especially where only relatively few fields of view are clear enough to be retrievable. The fact that mesoscale events have a spatially oriented structure makes it difficult to incorporate horizontal correlations objectively. The research to be done in this area almost amounts to objective pattern recognition.

2.3 Statistically Conditioned Least-Squares

This method has lain fallow for many years[4]. The operational sounding groups[5] rely mainly upon direct correlation between recently observed radiances and radiosondes to provide retrieval coefficients, using radiance consistency checks as quality control. Various R & D sounding groups use more complicated schemes, which juggle meteorological parameters in a radiation transfer model until the calculated radiances nearly match the observed ones.

The regression approach has the advantage of being reliably correct on the average, but has the disadvantage of being unreliable for single unusual soundings and of lacking an underlying physical model for detailed optimization. The iterative approach has the advantage of handling the single unusual field of view with a physical model, but has the disadvantage of not incorporating statistical experience and of not explicitly minimizing the uncertainty in the retrieved parameters. In any physically modelled retrieval, there is a burden of effort on the user to formulate and verify all of its details, such as the instrumental radiance errors and the atmospheric absorption coefficients, with the reward of understanding and controlling them.

The basic equations for statistically conditioned pseudo-inverse least-squares retrievals are shown in Appendix A. This approach has the advantage of optimizing the retrieval within the constraints of both a physical model and a body of objective statistical experience. Its disadvantage are the limits of the linearized sensitivity models and the effort it takes to prepare the statistical cases and sensitivity functions in advance of the observations. It will be a research effort to extend the method to include strong radiative effects like clouds, and to prove that iterated retrievals are truely optimized.

3. Simulated VAS Soundings

The VAS Processor is still being developed for launch, but a few computations have been made of the retrieval capability of the VAS instrument. A study using global statistics has been completed and answers general questions about vertical resolution and residual errors in a VAS retrieval. Another study is underway to determine the impact of detailed mesoscale statistical experience upon the retrieval of gradients in severe storms.

3.1 Global Conditioning

Using 1200 globally distributed radiosondes and rocketsondes prepared by NOAA, we have completed a general study of:[6]

---

[4] *Inversion Techniques for Remote Sensing of Atmospheric Temperature Profiles,* Fleming, H. E. and Smith, W. L., from Fifth Symposium on Temperature, Washington DC, June 1971, 2239-2250.

[5] *The Use of Eigenvectors of Statistical Covariance Matrices for Interpreting Satellite Sounding Radiometer Observations,* Smith, W. L. and Woolf, H. M., JAS, vol. 33, 1976, pages 1127-1140.

[6] D. Chesters, in progress.

- Calculation of sensitivity functions for temperature and moisture as seen by the VAS channels
- Consistency of the radiation transfer properties of the VAS channels at different latitudes
- Vertical resolution limits of a VAS retrieval
- Impact of instrumental noise
- Residual errors after retrieval with and without statistical conditioning.

Figure 3 shows that VAS soundings using sensitivity functions and global statistics can reduce the residual uncertainty in clear-air retrievals to the specified limits on temperature and moisture (±2°K and ±25 percent, respectively) and that the retrievals would not reach those limits without the aid of statistical conditioning.

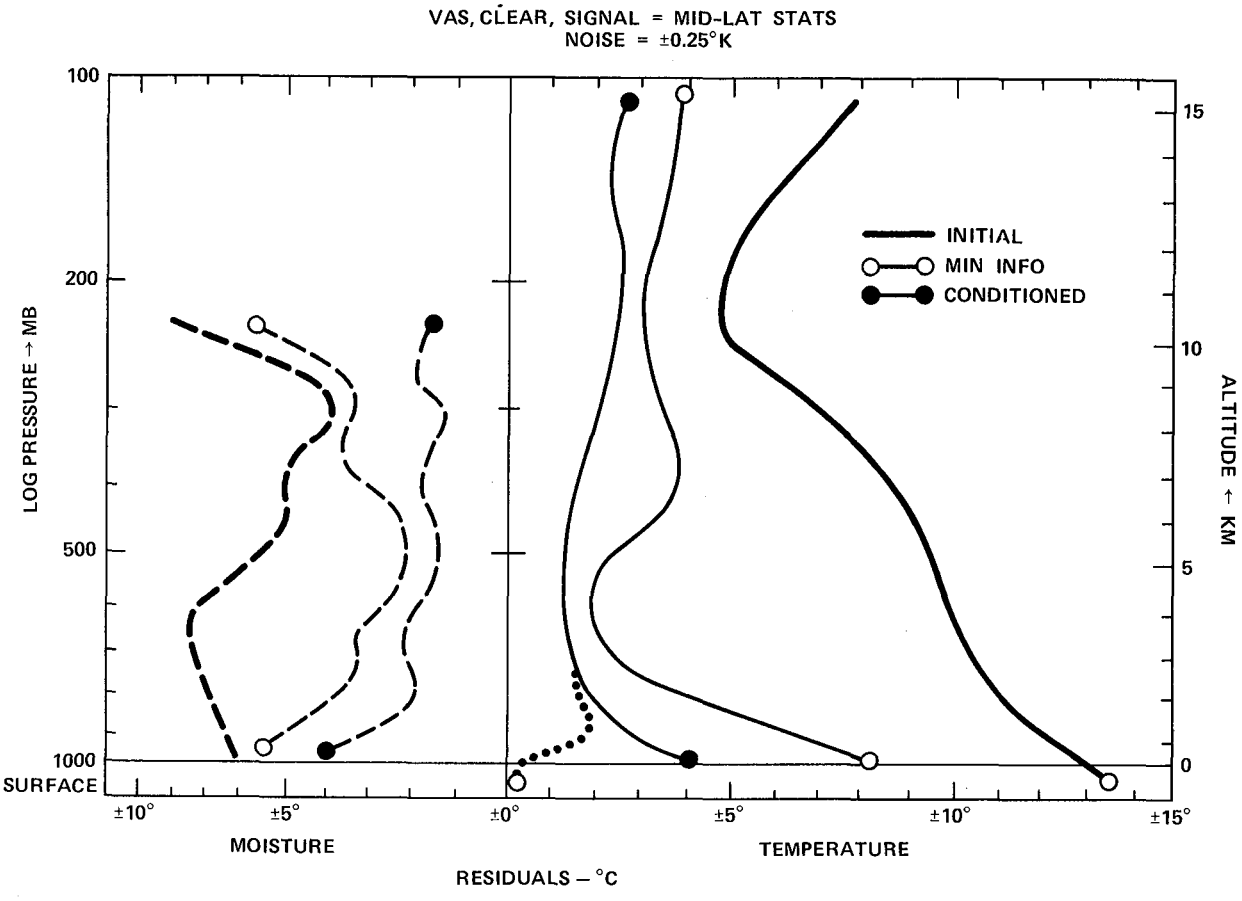

Figure 3. VAS sounding residuals for global simulations.

3.2 Severe Storm Conditioning

Using radiosonde reports from the NSSL stations reporting during severe storm outbreaks in Oklahoma during 1976, we are doing a detailed sounding study of the VAS retrievability of meso-scale gradients. Using six of ten cases, we have prepared mean and covariance profiles for "wet" and "dry" air masses. Radiance computations are underway for the remaining four of the ten cases, which will include cloud contamination. We will then retrieve the gradients from these four cases with both a regression scheme and a conditioned least-squares scheme to learn:

- General gradient retrievability
- Impact of "wet" and "dry" statistical subcategories
- Relative accuracy of each retrieval scheme for single fields of view as well as for the ensemble.

4. The VAS Software Sounding Laboratory

Because the statistically conditioned pseudo-inverse least-squares retrieval method controls so many elements of the inversion process, it supports the broader "software sounding laboratory" goal of the VAS Processor at NASA/GSFC. Reference profiles, sensitivity functions, radiance error models, meteorological experience, current ancillary data (first-guess profiles), and interactive iterated retrievals are all explicitly under the user's control. In addition, the algorithm shows promise for flexible extension to other meteorological situations, and to additional atmospheric parameters. Because it is an analytic method, it should also be possible to introduce physical quality control constraints, such as conservation laws or bounded parameters.

Appendix A
STATISTICALLY CONDITIONED LEAST-SQUARES RETRIEVALS

References 1–5 from the preceding pages each have some form of a statistically conditioned inverse in their own terms. Here, we will present the essential equations in simple notation.

Let X stand for a list of atmospheric parameters, such as temperature T(P), surface temperature T(S), dewpoint profiles D(P), cloud profiles, etc.

$$X(P) = [T(P), T(S), D(P)]$$

Let R stand for a list of observed radainces in all channels at one time and place.

$$R = R(\text{chan}, X)$$

Let lowercase letters stand for small variations in the variables in a linearized radiation transfer scheme:

$$R(\text{chan},X^0+x) = R^0(\text{chan},X^0) + r(\text{chan},x)$$
$$r(\text{chan},x) = dR^0(\text{chan})/dX^0(P) \cdot x(P) = Ax$$

where $A = dR^0(\text{chan})/dX^0(P)$ is the sensitivity function in the linearized matrix form.

Let r' be an observed noisy radiance.

$$r' = r + e$$

Let x' be the atmospheric variation estimated from a linear combination of observed radiance variations.

$$x' = Br' = BAx + Be.$$

Let S and E be the expected covariance matrices for the atmospheric and instrumental variations.

$$S = \langle x^2 \rangle, \qquad E = \langle e^2 \rangle$$

S and E are the "signal" and the "noise" learned from statistical experience.

Let Q be the expected residual variance.

$$Q = \text{SUM} \langle (x' - x)^2 \rangle$$

The minimization of the retrieved residuals Q with respect to the retrieval coefficiants B leads to the statistically conditioned least-squares pseudo-inverse.

$$B = SA'[ASA' + E]^{-1}$$

where A' is the matrix transpose of A.

The retrieval coefficients B are called a pseudo-inverse because both the ill-conditioned transfer problem and the introduction of measurement errors create a matrix that is not the identical inverse of the sensitivity functions A: $BA \neq 1$. However, the product BA does act as the information transfer matrix, since:

$$x' = Br' = BAx + Be \text{ implies } dx'/dx = BA$$

where dx'/dx is the response of the entire system (instrument plus algorithm) to a unit variation in the atmosphere.

Figure 4 shows the information transfer matrix for tropospheric temperatures T(P), surface temperature T(S), and tropospheric dewpoint-depression DPD(P). The estimate uses standard VAS sensitivity functions, global statistics, and nominal noise (±0.25°K per channel). The surface temperature is well determined in the absence of cloud or surface property uncertainties. The vertical resolution is approximately 5 kilometers, partly because of the strong vertical correlations in the global statistics. The low-level moisture profile is ill-determined due to the weak sensitivity of any VAS channel to low-level moisture.[7]

[7] D. Chesters, in progress.

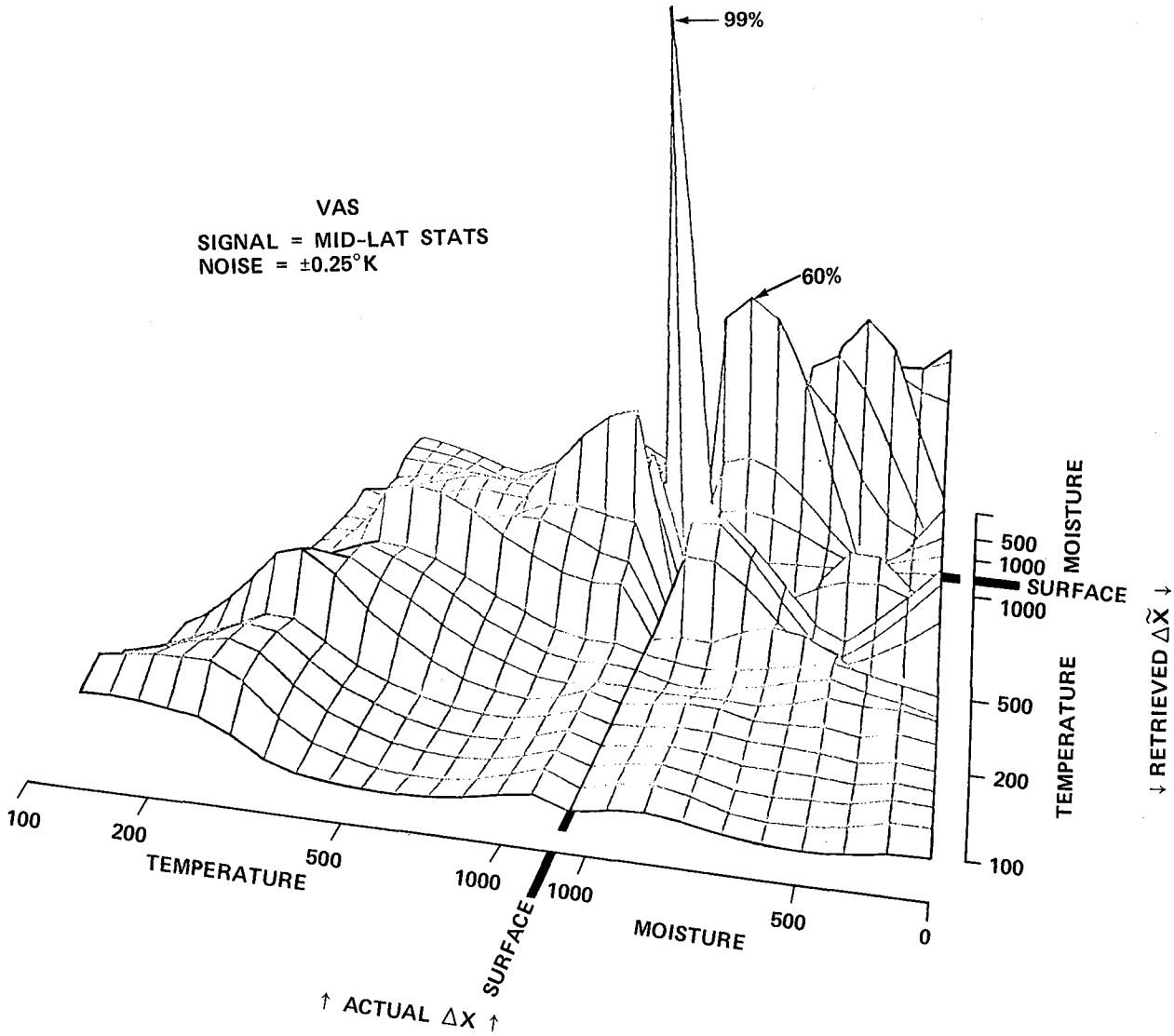

Figure 4. Estimated information transfer matrix for VAS.

GLOSSARY

FGGE	First Global GARP Experiment
FOV	Field of View
GARP	Global Atmospheric Research Program
GLAS	Goddard Laboratory for Atmospheric Sciences
HIRS	High-Resolution Infrared Radiometer Sounder
McIDAS	Man-Computer Interactive Data Access System
MSU	Microwave Sounding Unit
NESS	National Earth Satellite System (formerly National Environmental Satellite System)
NMC	National Meteorological Center
NOAA	National Oceanic and Atmospheric Administration
NSSL	National Severe Storm Laboratory
RAOB	Radiosonde Observations
SESAME	Severe Storm and Mesoscale Experiment
SSU	Stratospheric Sounding Unit
TOVS	TIROS-N Operational Vertical Sounder
VAS	VISSR Atmospheric Sounder
VISSR	Visible and Infrared Spin Scan Radiometer
VTPR	Vertical Temperature Profile Radiometer
TIROS	Television Infrared Observational Satellite
UW	University of Wisconsin

BIBLIOGRAPHIC DATA SHEET

1. Report No. 2157	2. Government Accession No.	3. Recipient's Catalog No.
4. Title and Subtitle VAS Demonstration Workshop – The Proceedings of a Satellite Sounding Workshop held July 15, 1980 at the NASA/Goddard Space Flight Center, Greenbelt, Md.		5. Report Date July 15, 1980 6. Performing Organization Code
7. Author(s) Editors: Daniel L. Endres and Louis W. Uccellini		8. Performing Organization Report No.
9. Performing Organization Name and Address NASA/Goddard Space Flight Center Greenbelt, Maryland 20771		10. Work Unit No. 11. Contract or Grant No. 13. Type of Report and Period Covered Workshop Proceedings 7/15/80
12. Sponsoring Agency Name and Address Harry Montgomery OSIP/VAS Demonstration, Code 942 NASA/Goddard Space Flight Center		14. Sponsoring Agency Code
15. Supplementary Notes		

16. Abstract

This report documents the presentations at the VAS Demonstration Sounding Workshop held at Goddard Space Flight Center on July 15, 1980. Seven papers were presented to review operational sounding techniques, discuss problems with collocation concept and cloud correction techniques, evaluate TIROS-N soundings within the operational analysis scheme and FGGE special effort, and propose new techniques for retrieving moisture and temperature profiles from TIROS-N and VAS radiance measurements.

17. Key Words (Selected by Author(s))	18. Distribution Statement
Operational Retrieval Methods, TIROS-N Soundings, FGGE Special Effort, VAS Soundings	

19. Security Classif. (of this report)	20. Security Classif. (of this page)	21. No. of Pages	22. Price*
Unclassified	Unclassified		

*For sale by the National Technical Information Service, Springfield, Virginia 22151.